This is to certify that the
dissertation entitled
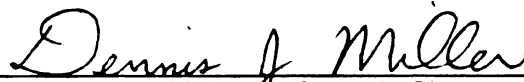
STUDIES IN THE HYDROGENATION OF BIORENEWABLE
FEEDSTOCKS

presented by

Ketan Pradeep Pimparkar

has been accepted towards fulfillment
of the requirements for the

Ph. D.   degree in   Chemical Engineering

Major Professor's Signature

2/27/09

Date

PLACE IN RETURN BOX to remove this checkout from your record.
TO AVOID FINES return on or before date due.
MAY BE RECALLED with earlier due date if requested.

DATE DUE	DATE DUE	DATE DUE

STUDIES IN THE HYDROGENATION OF BIORENEWABLE FEEDSTOCKS

By

Ketan Pradeep Pimparkar

A DISSERTATION

Submitted to
Michigan State University
In partial fulfillment of the requirements
for the degree of

DOCTOR OF PHILOSOPHY

Chemical Engineering

2009

ABSTRACT

STUDIES IN THE HYDROGENATION OF BIORENEWABLE FEEDSTOCKS

By

Ketan Pradeep Pimparkar

Proteins and amino acids are studied as feedstocks for catalytic hydrogenation to value added chemicals. A literature survey is presented describing the extreme conditions required for hydrogenation of the carbonyl functionality in such feedstocks. Three approaches tried out include hydrogenation of the peptide bond in dipeptides, hydrogenation of hydrolyzed proteins (oligopeptides) to polyaminoalcohols, and hydrogenation of amino acid mixtures. Challenges and interesting results obtained are discussed. In particular, the aqueous phase hydrogenation of amino acid mixtures was found to follow Langmuir-Hinshelwood type behaviour, with competitive adsorption between the amino acids for active sites on the catalyst surface.

Mass transfer resistances often play a limiting role in gas-liquid-solid reactions. Catalytic hydrogenations are such a class of reactions where high operating pressures and mechanical stirring are used to overcome these resistances. A novel PDMS based high pressure microreactor system was developed to enable the study of intrinsic kinetics of hydrogenation reactions under conditions where hydrogen is not the limiting reactant. A technique to immobilize catalysts within the microreactors was developed and used to study the aqueous phase hydrogenation of acetone. A kinetic model describes the results observed and sheds further light on the reaction mechanism.

Dedicated to my parents

ACKNOWLEDGEMENTS

Table of Contents

List of Figures

Caption

Key to Symbols

Species

A = amino acid A

$A \cdot S_1$ = adsorbed amino acid A

$A^{\bullet} \cdot S_1$ = adsorbed intermediate

Aol = amino alcohol from amino acid A

$Aol.S_1$ = adsorbed amino alcohol from amino acid A

B = amino acid B

$B \cdot S_1$ = adsorbed amino acid B

$B^{\bullet} \cdot S_1$ = adsorbed intermediate

Bol = amino alcohol from amino acid B

$Bol \cdot S_1$ = adsorbed amino alcohol from amino acid B

H_2 = molecular hydrogen

$H \cdot S_2$ = adsorbed hydrogen

P = phosphoric acid

S_1 = amino acid hydrogenation site

S_2 = hydrogen adsorption site

Variables

$\eta \varphi_j^2$ = observable modulus for species j

b = stoiciometric ratio of hydrogen to amino acid

C_j = concentration of species j, $kmol/m^3$

k'_j = surface reaction rate constant for species j, k_s / K_A, kmol/kgcat's

k_s = surface reaction rate constant, $kgcat^2/kmol^2 \cdot s$

K_A = adsorption coefficient of protonated amino acid A, $m^3/kmol$

K_B = adsorption coefficient of protonated amino acid B, $m^3/kmol$

K_P = phosphoric acid adsorption coefficient, $m^3/kmol$

K_{H_2} = adsorption coefficient of phosphoric acid $m^3/kmol$

$-r_A$ = reaction (consumption) rate of amino acid A, kmol/kgcat's

$D_{e,j}$ = effective diffusivity of species j, m^2/s

Chapter 1. Introduction

1.1 Background

Petroleum based products have become a part of all our daily lives. Petroleum products extracted from the earth are refined and used in a variety of applications, from transportation fuels to textiles and medicines. However, petroleum supplies, due to their non renewable nature, have been falling short of demand[1]. The resulting search for alternatives has identified plant and animal derived chemicals as potential substitutes. Starch, hemicellulose, cellulose, lignin, oils and proteins are some of the building blocks found in biomass feedstocks. Starch, oils and proteins are also important for nutritional purposes. As an example, corn, which is an important food source, can also be used to produce ethanol, a fuel, via fermentation. Research has therefore focused on using building blocks found in waste byproducts, such as cellulose, to produce fuels and chemicals. Byproducts from plant and animal processing - such as soybean meal and slaughter house waste - are rich in proteins (Table 1)[2]. They are currently used in low value applications such as fillers in feed for live-stock. Conversion of such waste proteins and their component amino acids into value added chemical products has been the primary objective of this work.

Proteins are made up of amino acids linked together by peptide bonds (Figure 1).
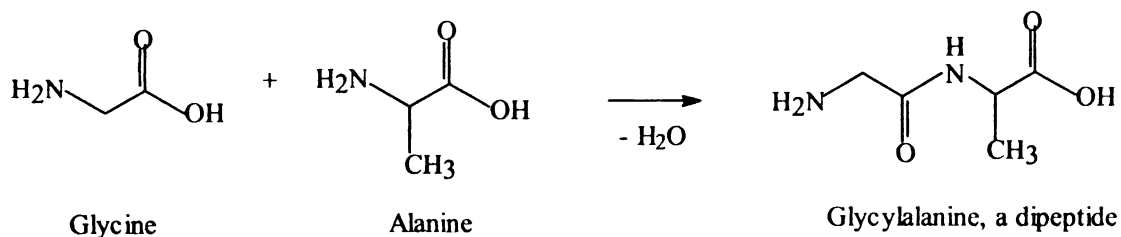
Figure 1 Condensation reaction between two amino acids to form a peptide linkage

Both the breakdown of proteins to amino acids and further conversion of the amino acids offer challenges. Hydrolytic cleavage of the peptide bonds can be accomplished using proteolytic enzymes or by using high concentrations of mineral acids in combination with high temperatures[3], yielding individual amino acids or peptide fragments. Amino acids obtained through such methods or via fermentation can be subjected to a number of processes such as hydrogenation, condensation, oxidation, esterification to enhance their utility as feedstocks [4,5] (Figure 2).
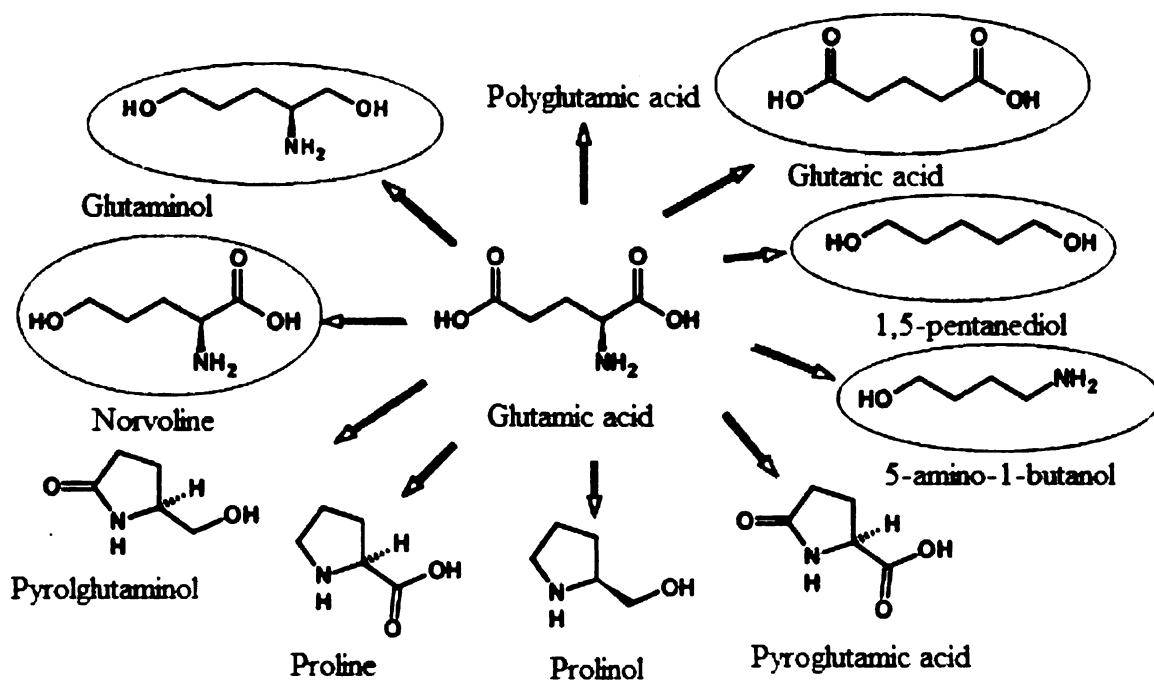
Figure 2 The large variety of transformations of glutamic acid which can yield useful products. Figure taken from PNNL report[5]

2

Table 1 General Characteristics Of Various Natural Feed Ingredients
Percent

	Dry Matter	Crude protein	Crude fat	Crude fiber	Total digestible nutrients		Digestable Protein Ruminants
					Ruminants	Swine	
Alfalfa meal, 20% dehydrated	93.1	20	3.5	20	58	50	14
Alfalfa meal, 17% dehydrated	93	17	3	24	58	32	12
Corn distillers dried solubles	93.8	27	9	13	79	92	19
Corn gluten meal	88	21	2	10	75	75	19
Cottonseed meal, solvent, 40%	91.4	41	4	13	71	67	33
Feather meal	93.2	85	2.5	1.5	63	63	70
Fishmeal, herring	93	72	10	1	73	70	57
Fishmeal, menhaden	92	62	10	1	71	62	49
Fishmeal, Peruvian	91	65	10	1	73	70	53
Meat and bone meal, 50%	92.6	50	8.5	3	68	65	40
Poultry byproduct meal	94	58	14	2.5	74	74	46
Sorghum grain	88.8	11	3	2	71	78	6
Soybean meal, solvent 50%	89.6	44	0.5	7	78	71	38
Soybean meal, 44%	89	15	4	10	62	57	11.5

Of the various processes available to upgrade amino acids and related biorenewable substrates, hydrogenation achieves a particularly large value upgrade. This thesis is divided into three main sections, each giving an account of the work done related to that topic. The first section describes attempts at hydrogenating polypeptides and proteins. Hydrogenation of amino acid mixtures forms the second part of the thesis, while in the third part we look at novel reactor configurations to carry out and study hydrogenations.

1.2 Significance

Conversion of proteins to value added products via hydrogenation requires reduction of the amide moiety present in proteins. Chapter 2 offers a brief literature survey of amide hydrogenations and proceeds to describe attempts at reduction of small molecule amides, oligopeptides and bulk proteins. Amides were found to undergo transamidation reaction with ethylenediamine as a solvent. This novel reaction opens up a route to the functionalization of amides, and offers possibilities for the manufacture of polymers incorporating amino acids. Hydrogenation of bulk protein hydrolyzates under conditions amenable to hydrolysis through use of inorganic acids led to the formation of desired product amino alcohols. However, quantitative characterization of the reaction mixture posed unique challenges and these are highlighted. This is one of the first reports studying conversion of proteins to value added feedstocks for the chemical industry and summarizes challenges likely to be encountered in further development of this route.

4

Given that amino acid substrates will likely come from complex mixtures arising from protein hydrolysis, it is important to study how the presence of multiple amino acids can influence hydrogenation rates of the individual species. Hence Chapter 3 discusses the hydrogenation of three amino acids: alanine, serine and valine and their mixtures. The hydrogenation of amino acid mixtures was found to follow Langmuir Hinshelwood type behaviour, with competitive adsorption between the amino acids for active sites on the catalyst surface. This information allows for improved understanding of substrate-catalyst interactions in such reactions and allows for more robust design of processes employing such conversions.

The drive towards more environmentally friendly processes translates to the need to use benign solvents such as water as widely as possible. In the case of aqueous phase catalytic hydrogenations, the low solubility of hydrogen in water and the high gas-liquid mass transfer resistance result in the need for extreme pressures and mechanical agitation to improve yields. Even so, in a majority of such reactions, hydrogen is found to be the limiting reactant on account of reduced availibility at the catalyst surface. Therefore, there was interest in developing an apparatus that allows study of aqueous phase catalytic hydrogenations under conditions where hydrogen is not the limiting reactant. Chapters 4 and 5 address this problem by detailing the development and use of PDMS-based microchannel systems to study high pressure hydrogenations. In Chapter 4, a PDMS-glass microreactor is incorporated into a high pressure hydrogenation setup. A novel technique to immobilize catalysts in PDMS microchannels is reported in Chapter 5, along with data that allow comparison of catalyst behaviour in batch mode with that in microchannel flow mode. These studies are an important contribution to the fundamental

understanding of catalyst behaviour in high pressure aqueous phase hydrogenations. Additionaly, they are one of the few reported implementations of high pressure hydrogenations in microchannel systems and are well suited to scale up either as characterization tools or as low volume, low cost manufacturing processes.

To summarize, each of the chapters to follow represents a novel and original approach to tackle difficult and multidisciplinary problems along the path towards a sustainable chemical process industry. In each case, substantial progress towards a solution has been made. This work is thus a significant contribution to the interrelated fields of aqueous phase catalysis and biorenewable feedstock based processes.

References

1   Kerr R. A., Science, **2007**, *317*, pp.437.

2   Considine D. M. and Considine G. D., *Food and Food Production Encyclopedia,* Van Nostrand Reinhold, New York, **1982**.

3   Fountoulakis M., Lahm H. W., *Journal of Chromatography A,* **1998,** *826* 109–134

4   Varadarajan S., Miller D. J., *Biotechnol. Prog.,* **1999,** *15,* 845-854

5   Werpy T., Petersen G., eds., *Top Value Added Chemicals from Biomass Volume I— Results of Screening for Potential Candidates from Sugars and Synthesis Gas,* PNNL report, August **2004**.

Chapter 2. Hydrogenation of Amides

2.1 Amines – Industrial Uses and Market Size

The reduced availability of petroleum based feedstocks has resulted in shortage of raw materials for a wide variety of chemicals. Polyaminoalcohols, which are widely used in the cosmetics industry, are among those compounds which have been affected. Alternative routes for the manufacture of amino alcohols are thus in demand. Amino acids can be hydrogenated to amino alcohols under relatively mild conditions, and this offers a possible alternative route. Protein rich-hence amino acid rich-waste is abundantly available from sources such as crop and animal processing. Examples include soybean meal (obtained after extraction from soybean oil), distillers grain solubles (obtained after distillation of ethanol from fermentation broth), slaughterhouse waste, and spoilt meat. Such protein rich wastes can theoretically be hydrogenated to a mixture of amino alcohols. Three main approaches for doing so include hydrogenating the proteins intact, hydrogenation after hydrolysis to oligopeptides, and hydrogenation after hydrolysis to a mixture of individual amino acids. In the case of the first two approaches, reduction of the amide functionality becomes a necessity. In this section, we will look at attempts to reduce the amide bond in dipeptides because these are easier to characterize than oligopeptides.

The total market for amines in the United States for the year 2004 is estimated to have been worth \$1.9 billion, corresponding to a demand of 70 × 10^6 kg of amines[6]. Amines can broadly be classified into **lower aliphatic amines, fatty amines, alkanol amines, cycloaliphatic amines,** and **aromatic amines**[7]. **Lower aliphatic amines** are derivatives of ammonia with one, two, or all three of the hydrogen atoms replaced by

8

alkyl groups of five carbons or less. Examples of lower aliphatic amines include methylamines, diethylamines ($3.22 per kg), propylamines ($3 to 4 per kg) and amylamines. Such amines are important intermediates in the manufacture of solvents, surfactants, agricultural, textile, rubber, medicinal and plastic chemicals. Amines with higher alkyl groups are known as **fatty amines**. These are nitrogen derivatives of fatty acids, olefins, or alcohols prepared from natural sources, fats and oils, or petrochemical raw materials. Fatty amines are surface active compounds and thus find wide application as surfactants. **Alkanol amines** (mostly mono, di and tri – ethanolamines; MEA – $1.4 per kg) are chemical intermediates used largely in the manufacture of surfactants and in gas conditioning applications to remove CO_2 and H_2S impurities from gas streams. Fatty amines and ethanolamines are the largest amine types used in the detergent and cleaner markets. **Cycloaliphatic amines** are low cost organic intermediates, and these generally consist of a cyclic hydrocarbon structural component and an amine functional group external to that ring. Examples include cyclohexylamine, (with a market of several thousand MT per year, used in water treatment and rubber chemical applications, $0.69 per kg ($0.31/lb)), and derivatives such as 4-methylcyclohexylamine. **Aromatic amines** include aniline and its derivatives, diaminotoluenes, diarylamines, methylenedianiline, and phenylenediamines. They find wide use in dyes, antioxidants, explosives, and pesticides. The varied applications of amines underscore their importance, especially as specialty chemicals.

2.2 Hydrogenation of Amides to Amines – Literature Survey

The hydrogenation of amides to amines (scheme in Figure 3) was first reported by Adkins and Wojcik in 1934[8]. In dioxane as a reaction medium, with copper- chromium

9

oxide as a catalyst under 10 to 30 MPa. of Hydrogen at 448 to 523 K , they found that lauramide and heptamide gave 40 to 70 % yields of corresponding primary amines. They also achieved conversion of N-laurylpiperidine.

Amide $+ H_2 \longrightarrow$ Amine
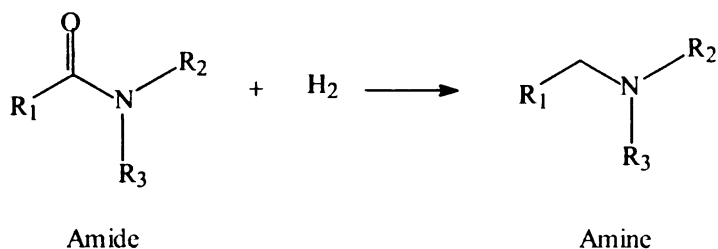
Figure 3. Reduction of amides to amines

Side reactions:

Amide $\longrightarrow$ Alcohol   Amine

Amine   Alcohol $\longrightarrow$ Byproduct amine $+ R_3OH$
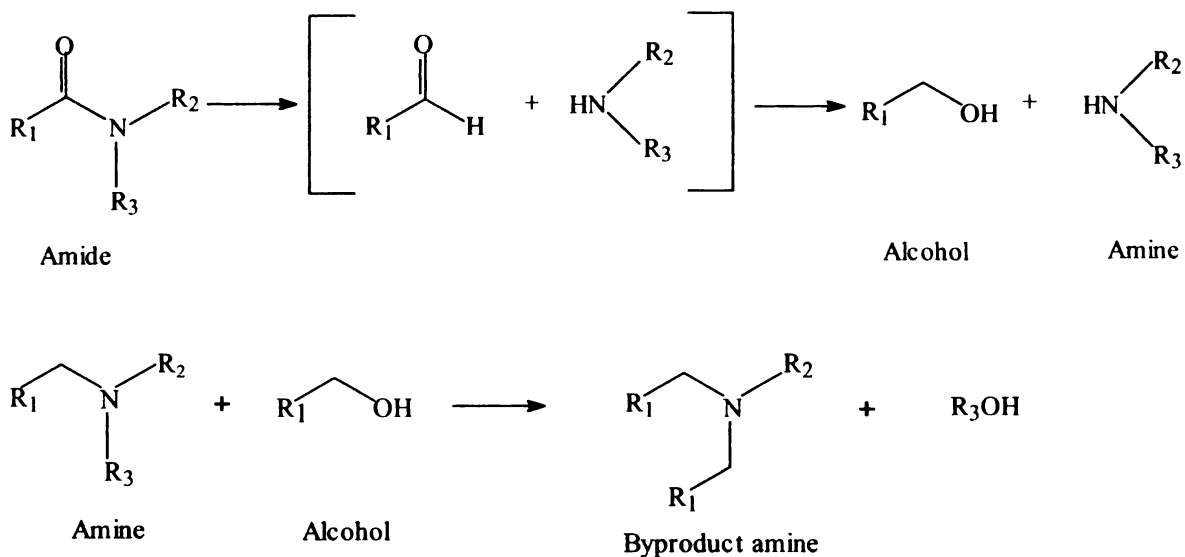
Figure 4. Side reactions in the reduction of amides to amines

The chief side reaction is the formation of secondary amines (Figure 4). The production of alcohols and mixed amines results in a requirement for distillation of the product mixture to isolate the desired product. This increases energy requirements. The reaction is favored by higher temperatures and higher pressures. The use of higher pressures implies customized equipment, increasing capital costs. The use of hydrogen, a flammable gas, at high pressures and temperatures poses a health and safety hazard. Better conversion can

10

be achieved by longer reaction times. In a batch setup, this implies the exposure of already formed product to high temperatures with the inherent risk of degradation. In the case of flow reactors, higher reaction times imply longer reactors.

Developments towards better efficiencies in this process have focused primarily on catalysts used in the process. Bard et al. in 1965[9] carried out the catalytic hydrogenation of N,N-disubstituted amides at 473 to 623 K, under 1.4 to 5.5 MPa of H_2 pressure using copper chromium oxide catalyst. Significantly, the presence of 2 to 8 wt % auxiliary dialkyl amine source was found necessary to increase attainable conversion. The auxiliary secondary amine source (same as that used to prepare the amide) inhibits the side reaction of conversion to alcohol. Best values reported are 90 % conversion, 81 to 88 % selectivity over 5 to 10 hrs. To utilize the enhanced reaction rates possible with higher surface area of catalysts, King, in 1984[10] used copper chromite supported on zeolite as catalyst. Hydrogen pressures of 1.3 to 3.4 MPa were required, although 72 % selectivity towards desired amines could be achieved in 1 hr. It was possible to omit the auxiliary dialkyl amine source. Mixed catalyst system of copper oxide, copper chromite and manganese oxide[11], palladium, ruthenium or rhenium supported catalyst and combinations[12], titanium based mixed metal oxide catalysts[13] have also been researched. The use of a nucleophilic reagent such as sodium methoxide in addition to the copper chromite catalyst has been found to reduce the pressures required to 0.5 to 2 MPa of hydrogen[14]. Bimetallic transition metal catalysts in homogeneous and heterogeneous forms reduced byproduct formation although typical reaction time required was 16 hrs[15]. The use of hydrosilanes as a hydrogen source eliminated the need for pressures.

Transition metal complexes as catalysts at 373 K, and reaction times approaching 16 hrs under inert atmosphere were required[16].

In 2006, in a significant step forward, Molengraft et al.[17] reported the aqueous phase catalytic reduction of the cyclic amide 2,5-piperazinedione to the cyclic amine 2,5–piperazine under relatively mild reaction conditions of 1800 psi hydrogen pressure at 130 °C over a period of 24 h, using Ru/C catalysts. However, linear amides such as glycylglycine do not undergo catalytic reduction under the same reaction conditions.

The challenges then are to increase conversion and selectivity in the hydrogenation of amides, including polypeptides, to amines. Different catalysts, solvents and reaction conditions are some aspects which can be optimized towards this end. A reasonable strategy would be to start with the hydrogenation of relatively susceptible molecules such as glycinamide, then move onto successively difficult molecules such as diglycine, triglycine and onto other oligopeptides. Glycinamide has been shown to be susceptible to hydrogenation[18].

2.3 Exploratory Studies in the Reduction of Amides

While the ultimate objective was to be able to hydrolyze and reduce proteins, it is difficult to characterize proteins because of their high molecular weight. Hence, polypeptides, smaller analogues of proteins, were chosen for study. Some examples of polypeptides include glycylglycine and glycylglycylglycine as seen in Figure 5 below.

Glycylglycine

Glycylglycylglycine
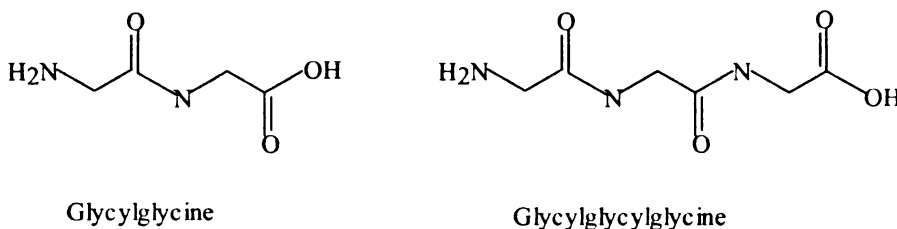
Figure 5. Examples of polypeptides.

In general, polypeptides are soluble in water, but are generally insoluble in any other solvent. In water, hydrolysis of the peptide bond giving constituent amino acids occurs far more readily than hydrogenation. Accordingly, our attempts at hydrogenation of glycylglycine under aqueous condtitions (100 ml solution volume of 0.22 M glycylglycine with 1 gm dry Ru/C under 6.9 Mpa hydrogen pressure and 130°C with stirring at 1000 rpm) resulted in complete hydrolysis to glycine and hydrogenation to ethanolamine, and no aminoethylethanolamine was observed. It was found that glycylglycine had excellent solubility (approx 20 wt %) in ethylenediamine. Reactions were therefore carried out using ethylenediamine as a solvent. Very few studies have reported the use of ethylenediamine as a solvent. Of these, one approach uses a reaction between fatty acids and amine to form polymers[19]. There have been no reported studies of amide hydrogenations using ethylenediamine as a solvent. Test reactions were carried out under standard hydrogenation conditions. Typically, 12 gm of substrate glycylglycine was dissolved in 140 ml ethylenediamine and added to 1 gm of prereduced 5 % Ru/C (dry basis). Each reaction involved subjecting the reaction mixture to 130°C and 7 Mpa hydrogen under stirring at 1000 rpm. Samples were withdrawn at regular intervals and subjected to analysis by nuclear magnetic resonance (N.M.R.) spectroscopy. Temperatures studied ranged from 100°C to 160°C. Reactions were carried out both with and without catalyst, and hydrogen pressures were varied from 0.1 to 6.9 Mpa. No desirable hydrogenation to aminoethylethanolamine was observed in these reactions.

The reactions did result in a transamidation reaction between the amide and solvent. Glycylglycine (glygly), glycine anhydride, and glycine were tested as substrates. As a test reaction, glygly was stirred in ethylenediamine at 1000 rpm for 7 hrs under 6.9

MPa hydrogen at 433 K, over 1.4 wt % catalyst (Ru on carbon, wet basis) in a Parr autoclave. NMR analysis showed that the glygly underwent a transamidation reaction with the ethylenediamine (Figure 6), with all the glygly forming N-(2-aminoethyl)glycinamide, as seen from H-NMRs and C-13 NMRs.
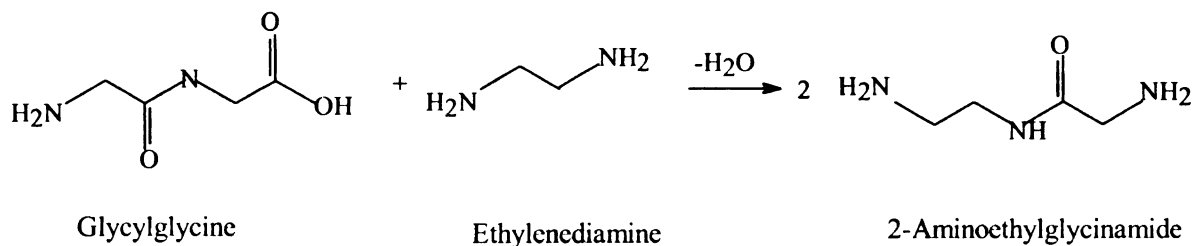
Figure 6. Transamidation reaction of glygly and ethylenediamine

Subsequently, a similar reaction was observed with glycine anhydride as substrate, under similar conditions. The absence of catalyst and hydrogen pressure also resulted in the same product with glygly. Thus, the transamidation reaction does not require catalyst or hydrogenation pressure. A control reaction was tried out with **glycine** as substrate, no catalyst, no hydrogen pressure. This, too resulted in amidation, albeit only at temperatures greater than 413 K. The results of the transamidation runs are summarized in Table 2.

Transamidation may offer novel routes to the synthesis of amines. Additionaly, the observed reaction opens up a route to potentially make polymers starting from amino acids or other organic acids.

Table 2. Results from studies of transamidation reactions.

Sr. no	Substrate	Solvent	H$_2$ pressure	Catalyst	Temperature	Time	Trans-amidation
1	12 gm glycylglycine	140 ml ethylenediamine	6.9 MPa	2.33 gm Ru on C (wet)	433 K	7hrs	Yes
2	1.3 gm glycine anhydride	140 ml Ethylenediamine	6.9 MPa	2.3 gm Ru on C (wet)	433 K	7 hrs	Yes
3	12.09 gm glyclyglycine	120 ml ethylenediamine	None, but sparged with H$_2$	No catalyst	433 K	7 hrs	Yes
4	5.58 gm glycine	120 ml ethylenediamine	None, but sparged with H$_2$	No catalyst	2 hrs 373 K, 2 hrs 393 K, 2 hrs 413 K, 7 hrs 433 K	-	Yes.

2.4. Protein Hydrolysis and Hydrogenation

Given the ready availability of cheap protein feedstocks from sources such as slaughter house waste, boven serum albumin (BSA) and commercially available whey hydrolyzate were chosen as substrates to study their potential utility as sources of chemical feedstocks. The approach taken was to hydrolyze the proteins or bulk hydrolyzates using either mineral acid such as H$_3$PO$_4$ or enzyme such as trypsin and then hydrogenate the hydrolyzate obtained.

Protein hydrolysis is a well studied subject, pursued primarily to discern the structure of proteins[20]. The standard procedure for breaking down a protein into its components involves dissolving the protein into a solution of 6 N HCl and heating the

same at 110°C for 24 hours. This results in a solution of the constituent amino acids which can then be analyzed to determine protein structure. Use of **inorganic acids** frequently results in the breakdown to the monomeric amino acids. Control of the reaction to achieve oligopeptides is difficult to achieve. **Enzymatic hydrolysis,** on the other hand, cleaves the protein at specific peptide bonds, such as alanine-serine, and thus results in a relatively more well-defined hydrolyzate solution. Both approaches were tried out, the objective being to obtain a solution of oligomeric amino alcohols.

2.4.1 Hydrolysis and Reduction Using H_3PO_4

Hydrogenation of amino acids to amino alcohols can be carried out using an acidic solution. The fact that proteins can be hydrolyzed in an acidic solution is thus advantageous, since a single pot reaction can theoretically be carried out. The protein BSA (Bovine Serum Albumin) was chosen as a substrate. This protein was subjected to hydrolysis and hydrogenation conditions in a Parr reactor. The resultant reaction mixture was analyzed using HPLC.

One gram of whey hydrolyzate was added to 100 ml water with vigorous stirring. 30 ml (85 wt %) H_3PO_4 was added to this suspension. The resulting suspension was transferred to a feed vessel. The feed vessel was then connected to a Parr reactor containing prereduced catalyst, 2.25 gm Ru on C (pre-reduced at 2.1 MPa hydrogen pressure, 523 K, for 10 h) and the feed was transferred to the reactor. The reaction conditions were 6.9 MPa of hydrogen pressure at a temperature of 428 K accompanied by stirring at 1000 rpm. The reaction mixture was sampled at 0 hr and 3 hrs. Samples were filtered over 0.22 micron Millex GV filters to remove catalyst particles. Reaction was stopped at the end of 4 hours, and samples were stored at temperatures below 277 K. The

significant quantity of phosphoric acid in the reaction mixture tends to leach nickel from the stainless steel reactor vessel. Hence, 20 ml of reaction sample at end of 4 hrs. was refluxed with $CaCO_3$ overnight to remove nickel. The resultant solution was filtered, the residue washed with water again, and the water was evaporated from the pooled solution, to give a white residue.

HPLC analysis of the reaction mixture (Figure 7 and 8) showed peaks corresponding to those of amino alcohols. Thus, some amount of the intended reaction products were obtained. However, analysis of high molecular weight peptide mixtures poses unique challenges, and these are discussed further towards the end of this chapter.

d:\dc\hplc disc\8thfeb\ethanolamine 2-8-05 1_38_32 pm.run
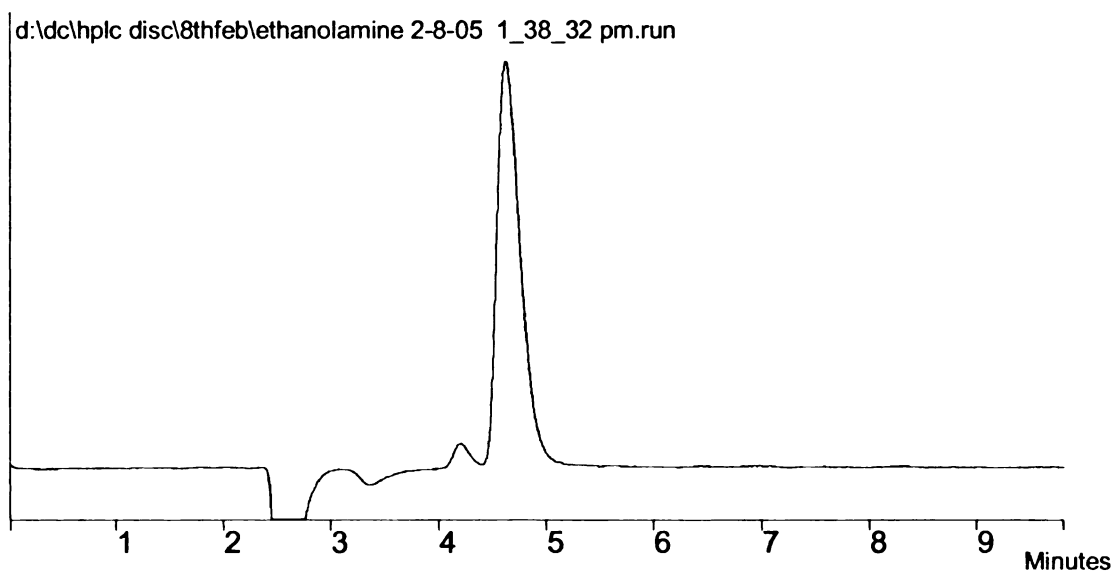
Figure 7. Chromatogram showing residence time of ethanolamine.
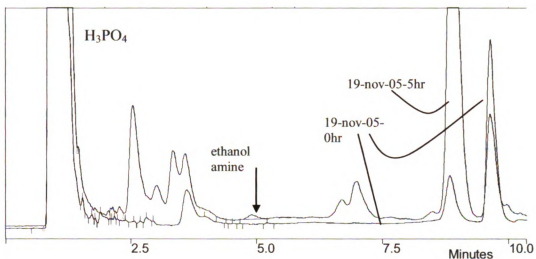
Figure 8. Chromatograms of initial and 5 hour samples from the whey hydrolysate hydrogenation reaction. There is a considerable increase in compounds eluting before 5 minutes. A peak in the general region of ethanolamine is observed in the 5 h sample.

2.4.2 Hydrolysis Using HCl Followed by Hydrogenation in a Parr Reactor

Hydrochloric acid is a stronger hydrolyzing agent than H_3PO_4. However, the corrosive nature of HCl prevents a one pot reaction from being carried out in the stainless steel Parr reactor. Instead, hydrolysis was carried out in a glass round bottom flask using 6 M HCl and the solution, after neutralization with NaOH, was hydrogenated. Apart from this separation of the hydrolysis step, the procedure was similar to that mentioned in the previous section. However, due to concerns related to degradation of the HPLC column, no analysis of samples from the reaction was attempted.

2.4.3 Enzymatic Hydrolysis using Trypsin and Subsequent Hydrogenation

Enzymatic hydrolysis of substrates enables mild reaction conditions (room temperature) and thus requires less energy input. Although enzymes cost more than mineral acids, enzymes can be immobilized onto supports, allowing their separation,

18

recovery and reuse. Experiments were therefore carried out using trypsin as a hydrolytic enzyme, with the objective of cleaving the protein BSA (Bovine Serum Albumin) into low molecular weigh fragments[21]. The resulting solution was subjected to hydrogenation in a Parr reactor, using a stoichiometric quantity of H_3PO_4.

Trizma-HCl (0.2586 gm) was dissolved in 40 ml water and 1 gm bovine albumin added to this. A solution of the enzyme was prepared by adding 0.01 gm trypsin to a 1 mM HCl solution. The 2 solutions were mixed, and kept at 313 K along with occasional shaking of the flask. At the end of 2 hours, a solution of 0.0053 gm trypsin inhibitor in 2 ml water was added to stop the hydrolysis. 10 ml of this solution was kept aside for analysis. The remaining approx 30 ml was hydrogenated as follows: 30 ml of the enzymatic hydrolyzate was diluted to 100 ml, 0.8 ml 85 wt % phosphoric acid was added and this was fed to the Parr reactor containing catalyst prereduced at 523 K, 2.1 MPa H_2 for 6 hrs. Subsequent hydrogenation conditions were 473 K, 6.9 MPa H_2, 1000 rpm for 6.5 hrs.

Gel electrophoretic analysis of the hydrolyzate before hydrogenation showed that the protein had not been hydrolyzed.

2.4.4 Results

The starting protein material had a high molecular weight (66000 daltons). Analysis of the protein hydrolysis was attempted using gel electrophoresis. Gel electrophoresis has the drawback that conventional techniques do not allow for determination of protein fragments with molecular weights less than 1000 daltons. Furthermore, this technique is not quantitative in nature. HPLC analysis of the reaction

mixture (hydrolysis and hydrogenation using H$_3$PO$_4$) (Figures 7 and 8) showed peaks corresponding to those of amino alcohols. Thus, some amount of the intended reaction products were obtained. However, accurate quantitative determination of the extent of hydrolysis and subsequent hydrogenation proved difficult.

To summarize, protein hydrolysis and subsequent hydrogenation do yield amino alcohols. However, quantitative analysis of the reaction mixture is difficult to achieve. Progress in this particular area will require close cooperation with experts in the analysis of high molecular weight biomolecules.

2.5 Summary

Attempts at hydrogenation of low molecular weight amides using ethylenediamine as solvent led to the discovery of a transamidation reaction between the substrate and solvent, but did not result in any reduction of the substrate. The transamidation of amino acids offers routes to the functionalization of amines and can also allow the incorporation of amino acids into polymers.

The hydrolysis and hydrogenation of oligopeptides and bulk protein hydrolyzates was attempted using inorganic acids and enzymes. In a single step reaction using phosphoric acid and under hydrogenation conditions, commercially available whey hydrolysate was found to yield ethanolamine. This is one of the first attempts at conversion of bulk proteins to value added chemical products.

Acknowledgements

References

6   US Amines Industry Serves Diverse Markets in Competitive Environment, Report by the Freedonia Group, 2000

7   Encyclopedia of Chemical Technology, vol. 2, Wiley, New York, 1991

8   H. Adkins. and B. Wojcik, *J. Am. Chem. Soc.*, vol. 56, pg. 247, 1934

9   N.M.L. Bard, Hopkins, Vertnik L., Fisher R., McCaleb K., US Patent 3190922, to General Mills Corporation, June 22, 1965

10   R. King, US Patent 448998, to The Procter and Gamble Company, May 15, 1984

11   C. Forquy and R. Brouard, US patent 5075505, to CECA SA, France, December 24th 1991

12   I. Dobson, EP0286280 A1, to BP Chemicals Limited, October 12th 1988

13   J. Barrault and M. Seffen, US Patent 4,935,546, CECA SA, June 19th 1990

14   M. Nepras, R Bernhardt. and C. Sporer, US Patent 5840985, Stepan Company, January 29th 1998

14   M. Nepras, R Bernhardt. and C. Sporer, US Patent 5840985, Stepan Company, January 29th 1998

15   C. Hirosawa, N. Wakasa and T. Fuchikami, *Tetrahedron Lett.*, **1996**, *Vol. 37, No. 37*, pp. 6749-6752

16   M. Igarashi, T. Fuchikami, *Tetrahedron Lett.*, **2001**, *Vol. 42, No. 42*, pp. 1945-1947,

17   A. Molengraft, M. S. Thesis, Michigan State University, East Lansing, MI, **2006**

18   Unpublished results, Miller Jackson group, Michigan State University

19   J. Cowan, L. B. Falkenberg, H. M. Teeter and P. S. Skell U.S. Patent 2450940 , 1948.

19   J. Cowan, L. B. Falkenberg, H. M. Teeter and P. S. Skell U.S. Patent 2450940 , 1948.

20   M. Fountoulakis and H-W. Lahm, *J. of Chromatogr. A*, **1998**, 826, pp. 109–134

21 T. Peters and R. Feldhoff, *Biochemistry*, **1975,** *Vol. 14, No. 15*, pp. 3384-3391

Chapter 3. Hydrogenation of Amino Acid Mixtures

3.1 Introduction

Catalytic hydrogenation of individual amino acids has been studied previously in our laboratory[22-25] and elsewhere[26,27]. As compared to traditional methods of amino acid reductions, viz. metal hydride catalyzed reductions, these methods use less hazardous and less expensive chemicals, produce no inorganic byproducts, eliminate the need for intermediate processing steps such as esterification, and allow the use of water as a reaction medium. Given that amino acid substrates will likely come from complex mixtures arising from protein hydrolysis, it is important to study how the presence of multiple amino acids can influence hydrogenation rates of the individual species. Hence we report here the results of a study of the hydrogenation of three amino acids: alanine, serine and valine and their mixtures (structures given in Figure 9a, representative reaction given in Figure 9b). The work is an extension of the prior work of Jere et al.[24,25] in which a rigorous kinetic model detailing active species, hydrogen pressure, and catalyst loading was developed. The goal of this work is to quantify reaction rates of the amino acids alone and in mixtures, to understand the competition between substrates and interactions between the substrates and catalyst, and to shed light onto the reaction mechanism. The understanding gained from this model system will aid in design of hydrogenation processes for more complex biorenewable feedstocks.

24

Serine   Alanine   Valine
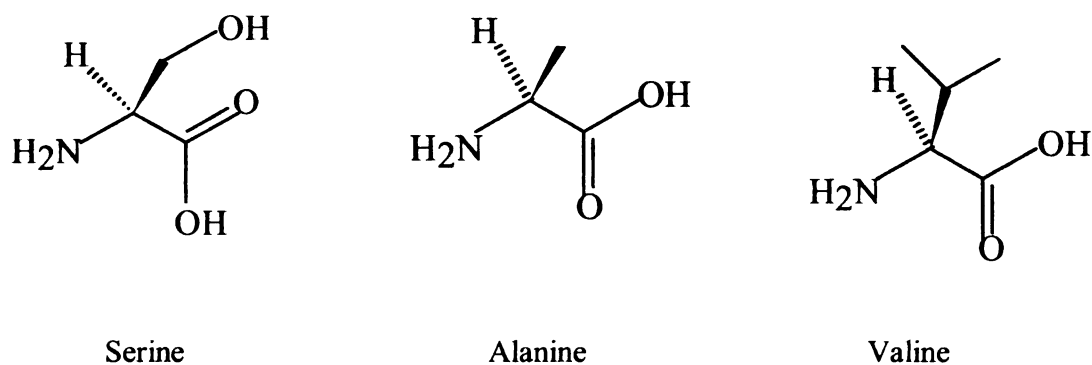
Figure 9a. Structures of amino acids

Zwitterion   Protonated   Alcohol
                     form
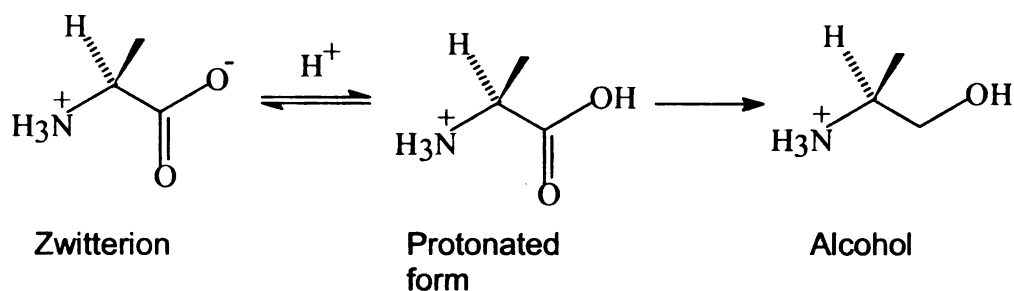
Figure 9b. Hydrogenation of alanine to alaninol

3.2 Hydrogenation of Organic Acids and their Esters – Literature Survey

Amino alcohols are used as chiral building blocks for a wide variety of specialty chemicals. The amino alcohols can be obtained by reduction of amino acids. Traditionally, such reductions have been carried out using metal hydrides such as sodium borohydride ($NaBH_4$) or lithium aluminum hydride ($LiAlH_4$). However, metal hydrides are hazardous, they need to be used in stoichiometric quantities, and they cannot be easily separated and reused. Heterogeneous catalytic hydrogenations offer the advantage of easy catalyst separation and reuse and thus allow the design of continuous processes.

25

Organic acids are not readily amenable to heterogeneous catalytic hydrogenations. Some of the earliest reports of catalytic hydrogenation of carboxylic acids to alcohols used copper catalysts at 573-673 K , 19.3 MPa hydrogen pressure[28], copper chromium catalysts[28,29] at 573 K and 24-35 MPa, copper cadmium catalysts[30] at 553 K and 11.7 MPa, copper-cobalt-nickel promoted catalysts[31] at 393-573 K and 3.6-38.6 MPa, ferrous metals modified with various non-ferrous chromites[32] at 473-673 K and 10-20 MPa, ruthenium dioxide[33] at 423 K and 48-56 MPa, rhenium black[34] at 423-473 K and 16-29 MPa. The hydrogenation of esters (Figure 10) in general requires milder conditions than those for the corresponding acid. Laszier[35] reported conversion of substrates such as n-butyl acetate over a mixed oxide catalyst containing copper, zinc and manganese, at 673 K and 20.7 MPa.

Subsequently, researchers have tried to reduce the severity of temperature and pressure conditions required for hydrogenation. These attempts have largely targeted catalyst optimization and solvent selection.
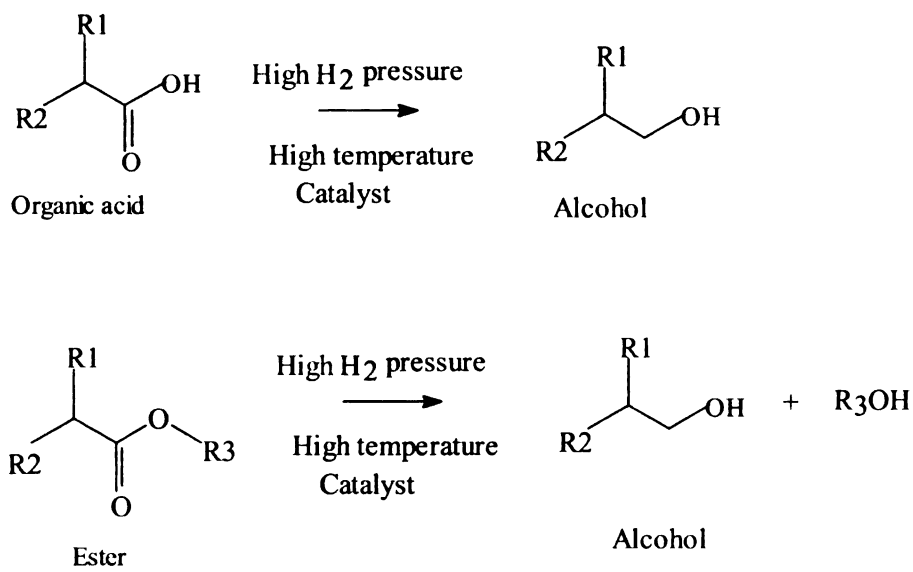
Figure 10. Schematic representing reduction of organic acid (R_3=H) and ester (R_3=alkyl) to alcohol

One of the earliest systems involving hydrogenation of esters studied was that of methyl formate to yield methanol. In the two step process of Christiansen[36], methanol was reacted with carbon monoxide to yield methyl formate which was subsequently hydrogenated to give net yield of one mole of methanol. Copper oxide reduced to copper was used as catalyst. Evans[37] studied the hydrogenation of methyl formate using copper chromite as catalyst, achieving 90% selectivity to methanol at atmospheric pressure and 373-503 K . The mechanism of methyl formate hydrogenolysis, as per Sorum and Onsanger[38], involves the formation of a hemiacetal intermediate, which is also the rate limiting step. The hemiacetal decomposes rapidly to formaldehyde and methanol, and the formaldehyde is hydrogenated to methanol (Figure 11).

$$CH_3O-CHO + H_2^* \longrightarrow CH_3O-CH(H^*)(H)(OH^*)$$

$$\downarrow$$

$$HCH_2OH^{(*)} + CH_3OH^{(*)} \xleftarrow{H_2^*} HCHO(H^*) + CH_3OH^{(*)}$$
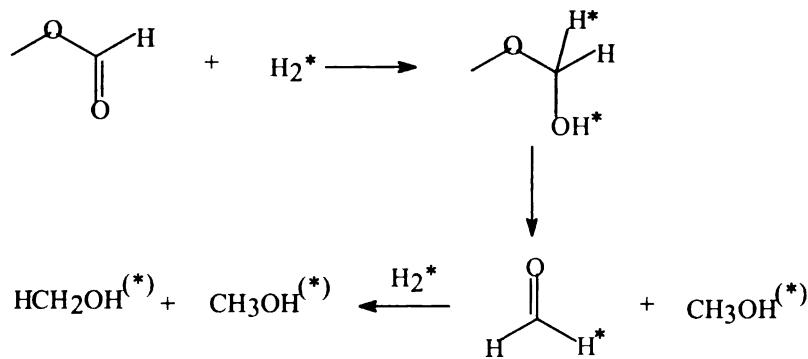
Figure 11. Mechanism for hydrogenolysis of methyl formate to methanol as proposed by Sorum and Onsanger[38].

Using in-situ IR spectroscopy and silica supported copper as catalysts, Trimm et al.[39] suggested that the formyl group is bound to the copper during hydrogenation.

Copper in the form of Raney Copper has been used to effect the hydrogenation of ethyl acetate (500 K, 4.8 MPa)[40], yielding ethanol. Formation of acetaldehyde, which is in equilibrium with ethanol, may limit conversion. Opportunities exist for innovative separation processes. Ethanol can also be prepared by hydrogenation of methyl acetate, with ethanol and ethyl acetate as intermediates, using a copper catalyst[41].

Studying fluorinated and perfluorinated esters, Yan[42] et al. proposed that the hydrogenolysis of esters proceeds through a hemiacetal intermediate. They based this assumption on the trace quantities of hemiacetals and or or aldehydes observed at the end of the reaction. Larger quantities of intermediates, particularly the hemiacetal, occurred in the case of the hydrogenolysis of fluorinated esters, since fluorinated hemiacetals are known to be stable. Additionally, they pointed out that the acetates were likely to

28

dissociatively adsorb to the catalytic surface via the acyl fragment[42]. Mechanistic studies have also been performed using isotopic labeling of methyl formate[43].

Adkins and coworkers[44] reported the low temperature (298-423 K) hydrogenation of esters to alcohols using modified raney nickel catalysts. In doing so, they improved on the work by Mozingo and Folkers[45,46] involving hydrogenation of malonates, acetoacetates, and benzoates using a high ratio of copper-chromium oxide to ester. By reducing the temperature and time of digestion of the raney nickel, they were able to achieve enhancement in catalytic activity towards hydrogenation of esters. With copper chromite, a high ratio of catalyst/substrate (1.5 gm of catalyst per gm of substrate) was sufficient for diethyl succinate, glutarate, adipate and methyl laurate - these were hydrogenated after 4 to 13 hrs at 423 K, even though they did not have any activating group. Raney nickel was active towards hydrogenation, yet all attempts to achieve selectivity w.r.t. phenol groups (avoid reduction of phenol group) did not succeed - cyclohexyl substituted alcohols were obtained as products. Amide linkages in a carboethoxy pyrrolidone and a hippurate were not hydrogenated while the ester group was being converted to a carbinol group, i.e. cyclic amide reduction was not observed. Beta substituted amino ester, ethyl beta piperidinopropionate underwent cleavage as the chief reaction with only a low yield of the desired piperidino alcohol. With alpha, beta hydroxy esters, hydrogenolysis was a problem. Difficulty of hydrogenating substituted malonates increased as the size of substituent increased. Adkins and coworkers also reported increases in reaction rates with increase in temperature and hydrogen pressure[47].

Hydrogenation of dibasic esters such as diethyl oxalate has been studied[38,48,49].
Catalysts used include Copper-Zinc oxide, silica supported copper and copper chromite.

Segel[50] studied hydrogenation of amino acid esters, revealing that copper chromite can give excellent yields of optically active amino alcohols, without the necessity of using large amounts of catalyst. Dioxane was used as a reaction medium. Esterification was carried out using the amino acid, ethanol and sulfuric acid. L-leucine ethyl ester was hydrogenated in 3hrs at 423 K, 1.38 MPa hydrogen pressure, giving 85% yield.

Broadbent et al.[34] studied the hydrogenation of organic acids using rhenium black synthesized in situ from rhenium heptoxide. They hydrogenated a wide variety of organic acids, such as acetic acid, capric acid, lauric acid, succinic acid to the corresponding alcohols. Solvent effects played an important role – while the hydrogenations run on the anhydrous acids always resulted in some by-product ester formation, those run in water as solvent gave markedly reduced ester formation, or in most cases no ester by-product at all.

Studer[51] et al. reported room temperature hydrogenation of chiral α-amino esters and α-hydroxy esters using a bimetallic nishimura catalyst and found no racemisation. The mixed Pt/Rh oxide, is generally active for ring hydrogenation. However, the authors chanced upon reduction of the carbonyl group during reduction of 2-hydroxy-4-phenyl butyrate. A relatively high loading of the catalyst was necessary – 10% (w/w) – lower catalyst loadings resulted in reactions but a variety of byproducts (dimmers and oligomers) were formed. Only the esters of α-hydroxy and α-amino acids were converted

– non functionalized esters, acids or amides failed to react. α-functionalised carboxylic acid derivatives could be selectively hydrogenated in the presence of another ester group, the non activated ester function remains unreduced but formed a lactam. Reactions with β-amino acid esters were slower than with the α-amino esters. Higher catalyst loadings were necessary for α-hydroxy esters than for α-amino esters. The catalyst had a different appearance in the low temperature experiments (finely divided powder), as compared to high temperature experiments (aggregates). Reuse of the catalyst was not possible. The addition of acid led to a significantly reduced reaction rate. The authors propose a multifunctional active centre consisting of a basic and multi-metallic sites. They theorize that the α-NH_2, α-NHR, or α-OH groups act as efficient anchoring groups by interaction with a basic site situated very close to the metallic centers leading to the strongly adsorbed and activated centre, with implications for the reactivities of α vs. β substituted esters.

Varga[52] et al. studied the effect of different electron withdrawing and hydrogen bonding or sterically hindering vicinal substituents on the carbonyl group of carboxylic acids (Figure 12). Both hydrogen bonding and electron withdrawing nature of the vicinal substituents was found to activate the substrate towards hydrogenation. The compounds studied included lactic acid (LA), glycolic acid (GA), 2-methoxypropanoic acid (MPA), methoxyacetic acid (MA), isobutyric acid (IBA), propanoic acid (PA), 2-chloropropanoic acid (2CPA), ethyl lactate (EL), 2-acetoxypropanoic acid (2APA). The order of reactivity towards hydrogenation at the carboxyl group was: PA < 2MPA < IBA < MA < GA < LA < EL. 2-acetoxypropanoic acid underwent hydrolysis to lactic acid and so the effect of the acetoxy group at the 2 position could not be studied. 1-chloropropanoic acid

converted to propanoic acid and did not undergo further conversion. They also propose a reaction mechanism proceeding through a hemiacetal, aldehyde and finally resulting in the alcohol.

Lactic acid (LA)

Glycolic acid (GA)

2-Methoxypropanoic acid (MPA)

Methoxyacetic acid (MA)

Isobutyric acid (IBA)

Propanoic acid (PA)

2-Chloropropanoic acid (2CPA)

Ethyl Lactate (EL)

2-Acetoxypropanoic acid (2APA)
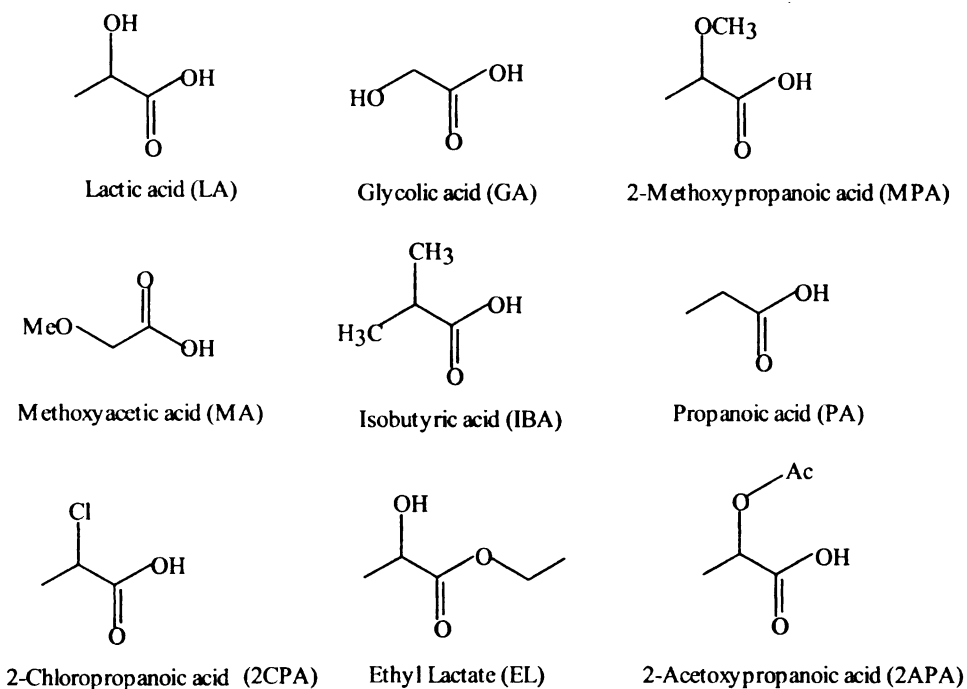
Figure 12. Substrates used by Varga et al. to study effect of vicinal substituents on rate of hydrogenation of carboxylic acids.

Zhang et al.[53] studied the aqueous phase hydrogenation of lactic acid to propylene glycol. They achieved 95% conversion at 373 to 443 K, hydrogen pressures of 7 to 14 MPa. Selectivity to propylene glycol was 90%. Potassium, calcium lactate salts cannot be directly converted to PG, however, addition of sulfuric acid converts the salts to calcium, potassium sulfates and allows hydrogenation. Lactic acid is expected to be available cheaply ($0.85/lb), hence this route can compete with traditional route for manufacture of

PG. Traditional routes to propylene glycol involve hydroperoxidation or the chlorohydrin process. Pervious work by Adkins[44] (25 MPa, high catalyst loading), Broadbent[34] (hydrogenation of free lactic acid using unsupported rhenium black as catalyst, 8h, 423 K, 27 MPa), Ford, Carnahan[33] (Pressures > 48 MPa for direct hydrogenation of carboxylic acids) relied on high hydrogen pressures. In comparison, the work by Zhang et al. offers higher reaction rates, better selectivities under milder conditions. At temperatures greater than 443 K, byproducts such as propanol and ethanol were formed. As stated earlier, the salts need to be acidulated prior to hydrogenation.

Patents by Antons et al.[54,55] and work by Jere et al.[56,57] revealed that the use of inorganic acid allowed the conversion of amino acids to the corresponding amino alcohols at relatively mild conditions of temperature and pressure (373 K, 6.9 MPa hydrogen), with stereoretention (Figure 13, 14) .

Jere also found rapid H-D exchange at the C2 position without loss of stereochemistry and without any reaction in the hydrogenation of alanine. In addition, stereoretentivity was observed at temperatures as high as 383 K.
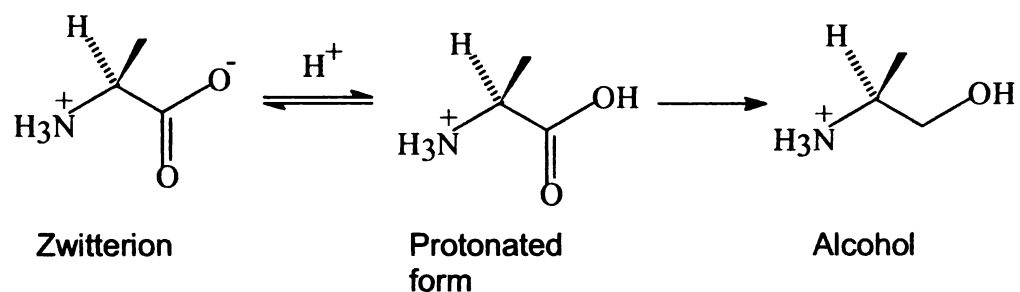
Figure 13. Amino acid hydrogenation on addition of inorganic acid – the inorganic acid converts the amino acid to its protonated form.

33
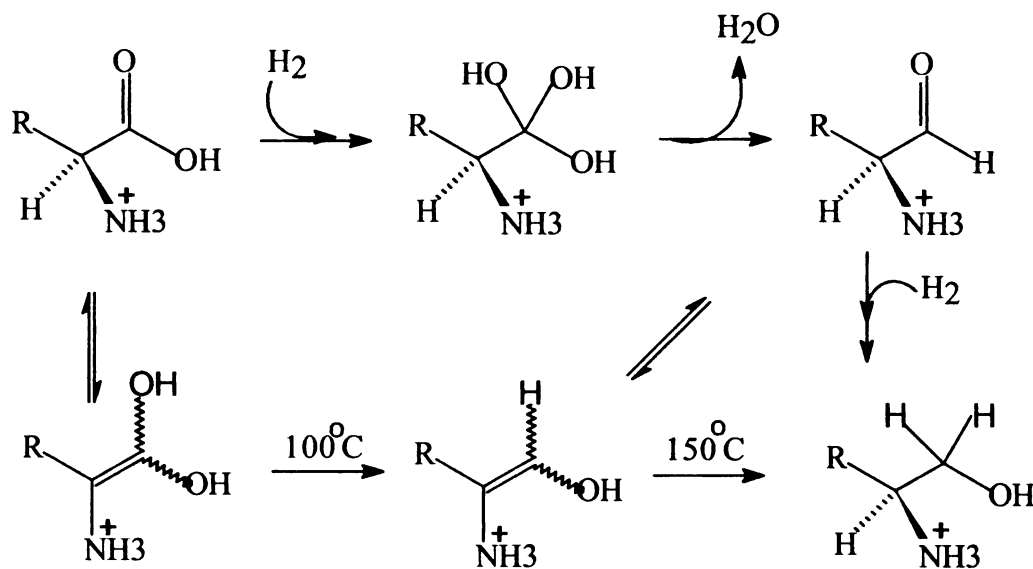
Figure 14. Generalized amino acid hydrogenation sequence showing aldehyde and potential enols as proposed by Jere et al.[30]

Recent work by Chen et al.[58] has shown that competition for catalyst active sites exists between lactic acid and propionic acid during the course of their hydrogenation. In their case, addition of a second acid significantly decreased the conversion rate of the first acid. A Langmuir - Hinshelwood type mechanism was able to predict the reaction kinetics. Lahr and Shanks[59] have also looked at competitive adsorption during hydrogenation with glycerol, ethylene glycol and propylene glycol.

3.3   Materials and Methods

Aqueous phase catalytic hydrogenation of amino acids was carried out in a Teflon-lined 300ml Parr high pressure reactor (Model 4560). Alanine, serine, valine, and HPLC-grade water were used as purchased from Sigma-Aldrich. The catalyst was a pre-

reduced 5% ruthenium on carbon (Johnson Matthey - Tennesee, lot no. 20892), obtained as a slurry containing approximately 50 wt% water.

To begin a reaction, 1.0 g of 5 wt% Ru/C catalyst (dry basis) was added to the dry reactor. The reactor was flushed to remove air, and then the catalyst was reduced under 1.5 MPa hydrogen and 200°C overnight. The reactor was then cooled to room temperature, a solution of amino acid substrate in 100 ml water was added to the reactor under low hydrogen pressure, and the stirring rate was fixed at 1000 rpm. Because hydrogenation of amino acids requires that they be present in the protonated form, a slight molar excess (10–20%) of phosphoric acid (relative to the amino acid) was added to the feed solution in each reaction prior to reaction. When the reactor temperature stabilized at the desired value (363-403 K), the reactor was pressurized with hydrogen gas (7 MPa) to initiate the reaction (t=0). Samples (1 to 2 ml) were withdrawn at regular intervals through a sample loop, filtered using Millipore Millex GV syringe filters, diluted in water to ~0.005M, and analyzed on a Waters HPLC with ultraviolet (UV) and Evaporative Light Scattering (ELS) detectors using a reverse phase ion exchange column from Silec Technologies[21]. The HPLC method employed an acetonitrile/trifluoroacetic acid (TFA)/water gradient as follows: the binary gradient shifted linearly from a 0.05% TFA - 10% ACN solution (mobile phase A) in water to a 0.5% TFA - 10% ACN solution in water (mobile phase B) over 12 minutes, and then the latter mobile phase continued for an additional 18 minutes. A ten minute equilibration time on mobile phase A was included in each run before the next sample was injected. Five-point calibration curves were obtained for each compound at concentrations from 0.0005M to 0.005M. The

solubilities of the substrates in water at 28°C are listed in Table 3. The concentrations used for all experiments were well below these maximum values.

Table 3. Solubilities of amino acids in water at 25°C [60,61]

Amino acid	Solubility in water (g/100g, 25 °C)	Solubility (M)
Alanine	16.6	1.9
Valine	8.85	0.8
Serine	50.23	4.8

The calibration curves for the ELS detector are non-linear at lower concentration ranges, but were reproducible in repeated calibrations. The combined ELSD chromatogram for all three amino acids and their alcohols is given in Figure 15. Only the alaninol and valine peaks show significant overlap – these species concentrations were determined by integrating the UV peak for valine (alaninol has no UV signal) to determine valine concentration, then subtracting the corresponding valine area from the combined ELSD peak to give an alaninol peak area and thus the alaninol concentration. We attempted a direct deconvolution of the valine – alaninol overlapping peaks, but this procedure yielded significantly less reliable results compared to the UV/ELSD measurements. Concentration changes over the course of the reaction were thus obtained from the HPLC data and were used to calculate conversion, product yields, selectivities, and overall material balances. Fractional conversion was calculated relative to the concentration of amino acid in the solution added to the reactor – in some instances

(Figures 16, 19, 20), the conversion of the reaction sample taken upon reaching steady state conditions (t = 0) is less than zero, because of either uncertainty in the analysis or evaporation of water in the reactor that results in artificially high concentrations. In no case was the conversion less than -4%.
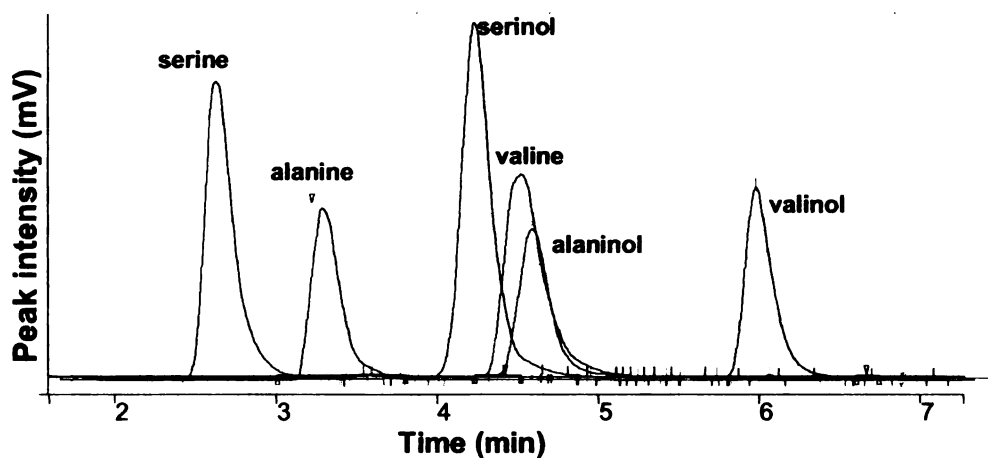
Figure 15. Composite HPLC chromatogram of ELSD detector signal showing individual peaks of compounds studied.

3.4 Results and Discussion

3.4.1 Hydrogenation of Individual Amino Acids

Serine, alanine and valine were hydrogenated at 130°C and 7.0 MPa H_2 over concentration ranges from 0.12 M to 0.5 M with 5 to 20 per cent excess H_3PO_4. As can

37

be seen in Figure 16 for a 0.46 M feed solution of the amino acid with 0.5M H_3PO_4, serine and alanine react significantly faster than valine. The same trend was observed when the acids were reacted at an initial concentration of 0.22 M, with serine and alanine conversion nearly complete by the end of 3.5 hrs.
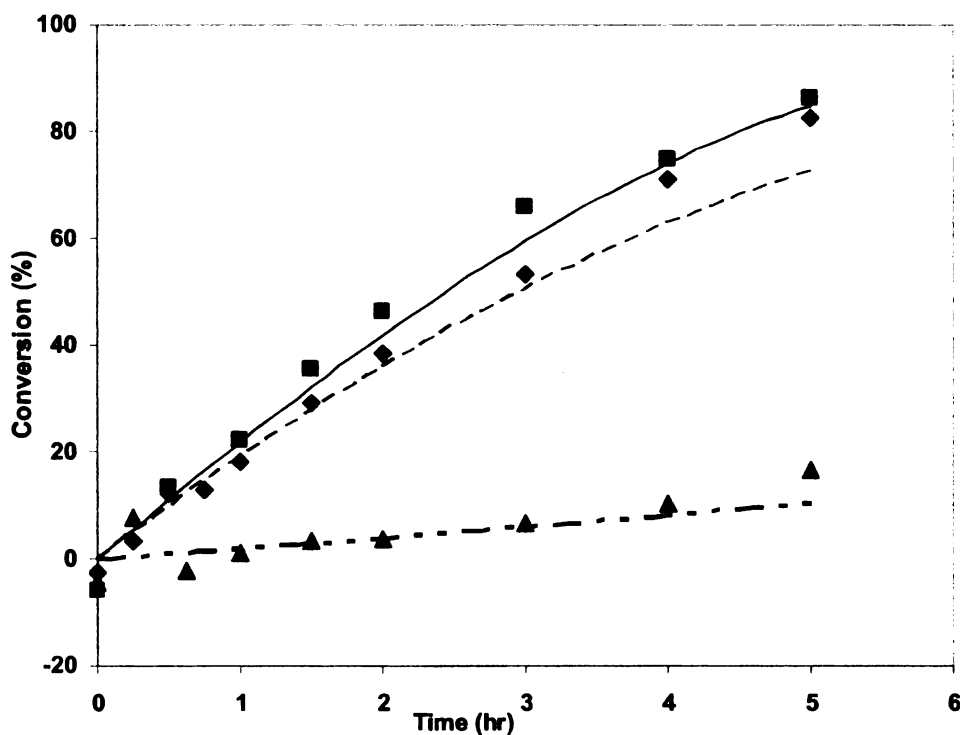
Figure 16. Hydrogenation of serine, alanine and valine at 130°C and 7.0 MPa hydrogen pressure. (■) - 0.48M serine + 0.52M H_3PO_4; (♦) - 0.46M alanine + 0.5M H_3PO_4; (▲) - 0.49M valine + 0.5M H_3PO_4. Conversions predicted by the model are represented by the lines as: _____ 0.48M serine + 0.52M H_3PO_4 ; .... 0.46M alanine + 0.5M H_3PO_4 ; _..._ 0.49M valine + 0.5M H_3PO_4

For alanine and valine, carbon molar balances closed to 96% ± 4%, and both alanine and valine showed greater than 90% selectivity to their corresponding amino alcohols. In contrast, liquid phase carbon molar recovery in serine hydrogenation was

only 70%. A control reaction (130°C, 7.0 MPa H_2) starting with serinol and H_3PO_4 resulted in 26% serinol degradation over 5 hr. At these temperatures, methane and ethane were observed as byproducts in GC-MS of the vapor phase. Thus, serinol degradation leads to lower than anticipated selectivity to serinol and lower mass balance closure in serine hydrogenation than with the other amino acids.

Concentration profiles versus time were plotted for each reaction and fitted to a second-order polynomial. Differentiation of the resulting curves allowed calculation of rates at various times over the course of reaction. Initial rates were thus calculated by evaluating the slope of the curve at time zero. By incorporating the acid concentration and the quantity and properties of the catalyst, reaction rates on a catalyst mass basis (kmol acid/kg catalyst/s) or on a reactor fluid volume basis (kmol acid/m^3 solution/s) were determined. These initial rate data were used to estimate the activation energy and the dependence of rates on acid feed concentrations. This initial rate evaluation minimized possible complications from side reactions and catalyst deactivation.

Initial hydrogenation rates at different feed concentrations for serine, alanine, and valine (approximately 0.15, 0.22, and 0.5 M) with otherwise identical reaction conditions are reported in Figure 17. The reaction rates for serine and alanine exhibit a non-linear dependence on initial concentration, and thus the hydrogenation reactions are not first order with respect to the amino acid concentrations. This observation is consistent with the results obtained by Jere et al.,[56] who reported a Langmuir-Hinshelwood rate expression describing the reaction kinetics of alanine hydrogenation. Valine reaction rates were zero order in valine concentration over feed concentration ranges 0.02 M to 0.5 M.

Activation energies for amino acid hydrogenations were estimated by plotting the natural logarithm of the initial rate versus reciprocal absolute temperature at constant initial concentration and catalyst loading (Figure 18). The activation energies reported in the caption are similar for the three amino acids; the value for alanine (81.5 kJ/mol) is in reasonable agreement with the value reported by Jere et al.[56,57] (86.4 kJ/mol) in earlier work.
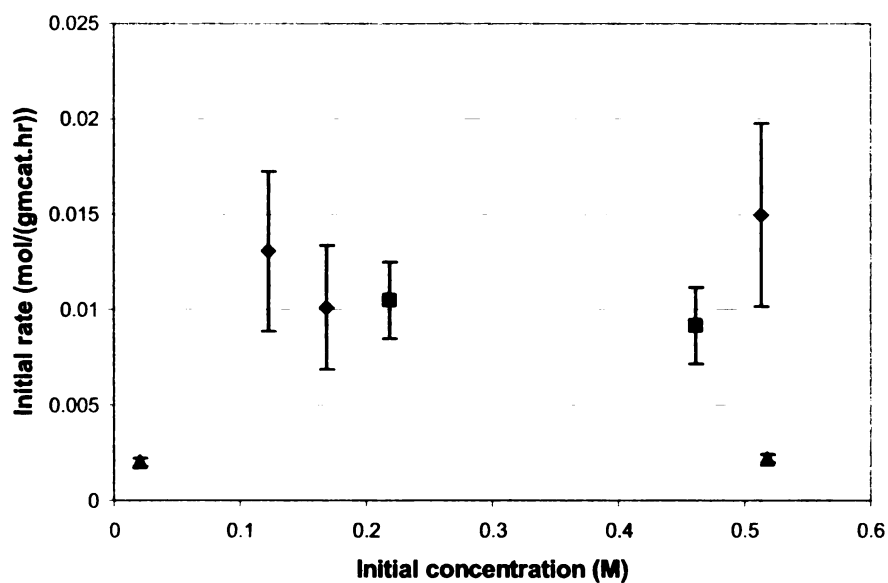
Figure 17. Effect of initial concentration on initial hydrogenation rates for the amino acids. (♦) – serine; (▲) – valine; (■) – alanine.
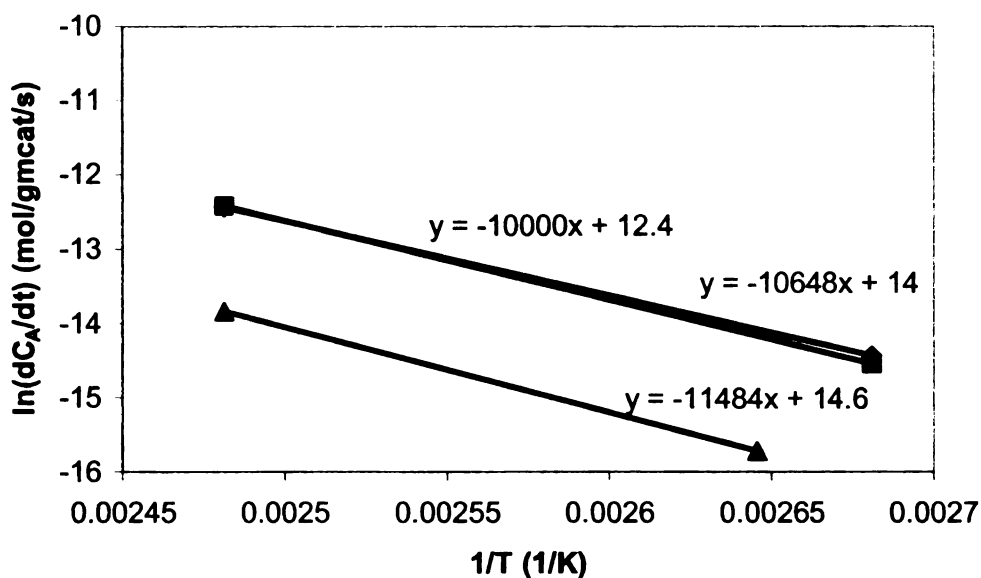
Figure 18. Arrhenius plot of rate constants for alanine, serine and valine hydrogenation. (♦) - serine, E_a = 83.1 kJ/mol; (■) - alanine, E_a = 88.5 kJ/mol; (▲) - valine, E_a = 95.5 kJ/mol.

3.4.2 Hydrogenation of Amino Acid Mixtures

Recent work by Chen et al[58] illustrates competition between lactic acid and propionic acid for catalyst active sites during hydrogenation. In that work, addition of a second acid significantly decreased the conversion rate of the first acid. A similar effect is observed in the case of hydrogenation of amino acid mixtures. As seen in Figure 19, addition of serine or valine to the feed at a fixed alanine concentration slows alanine hydrogenation increasingly as the concentration of the competing amino acid increases. A similar effect can be observed when alanine or valine is added to serine hydrogenation (Figure 20).

41
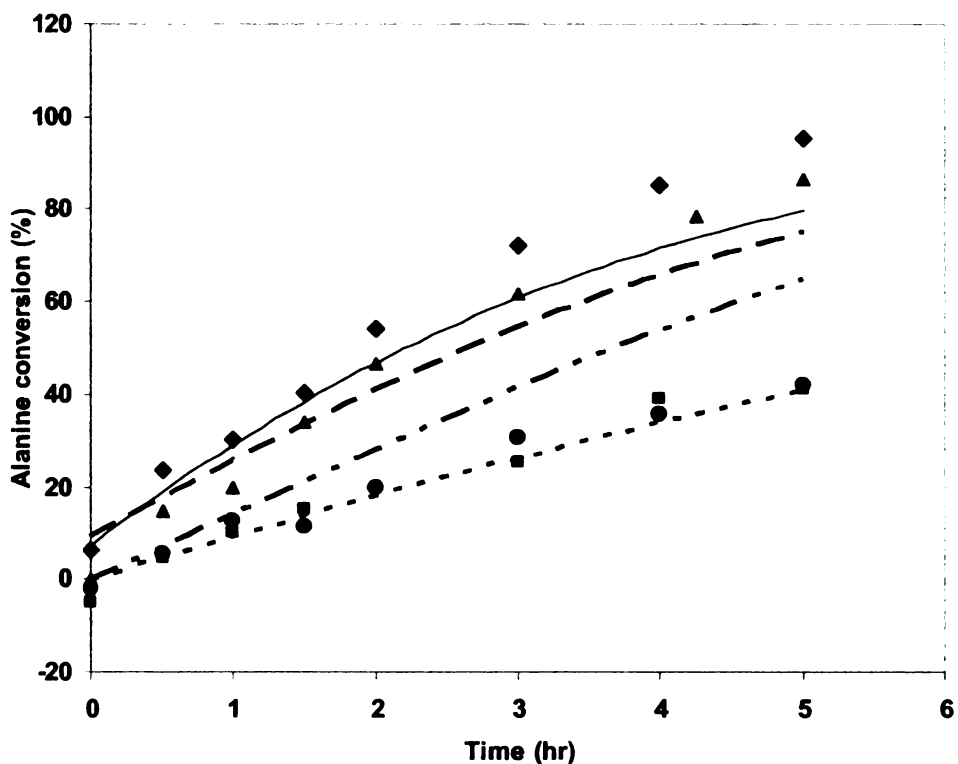
Figure 19. Hydrogenation rates of alanine alone and in mixtures with serine and valine at 130°C and 7.0 MPa hydrogen pressure. (♦) - 0.24M alanine + 0.56M H_3PO_4; (▲) - 0.22M alanine + 0.13M serine + 0.56M H_3PO_4; (■) - 0.23M alanine + 0.24M serine + 0.56M H_3PO_4; (●) - 0.22M alanine + 0.24M valine + 0.56M H_3PO_4. Conversions predicted by the model are represented by the lines as: _____ 0.24M alanine + 0.56M H_3PO_4; _ _ _ _ 0.22M alanine + 0.13M serine + 0.56M H_3PO_4; __ .. __ 0.23M alanine + 0.24M serine + 0.56M H_3PO_4; .... 0.22M alanine + 0.24M valine + 0.56M H_3PO_4
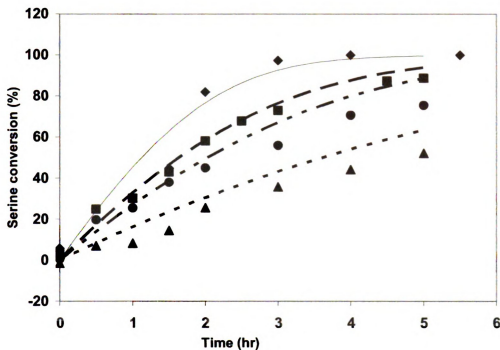
Figure 20. Hydrogenation of serine alone and in mixtures with alanine and valine at 130°C and 7.0 MPa hydrogen pressure. (♦) - 0.24M serine + 0.56M H_3PO_4; (■) - 0.48M serine + 0.52M H_3PO_4; (●) - 0.24M serine + 0.23M alanine + 0.56M H_3PO_4; (▲) - 0.24M serine + 0.25M valine + 0.56M H_3PO_4.

Conversions predicted by the model are represented by the lines as: _____ 0.24M serine + 0.56M H_3PO_4; _ _ _ _ 0.48M serine + 0.52M H_3PO_4; _ .. _ 0.24M serine + 0.23M alanine + 0.56M H_3PO_4; .... 0.24M serine + 0.25M valine + 0.56M H_3PO_4

3.4.3   Analysis of Mass Transfer Resistances

For the data to represent intrinsic kinetics of the reaction, the contents of the reactor must be well mixed and resistance to mass transfer should not limit the hydrogenation rate. Mass transfer in the reactor consists of the following steps: 1) hydrogen transport from the gas phase to the liquid phase across the gas-liquid interface; 2) hydrogen and alanine transport from the bulk liquid phase to the catalyst particle surface across the solid-liquid interface; and 3) hydrogen and alanine diffusion through the porous catalyst support to the metal surface sites. In addition, a prerequisite for

43

unhindered mass transport is that all catalyst in the reactor is suspended in solution. The Zwietering correlation[62] gives an estimate of the minimum stirring rate necessary for complete catalyst suspension. For this system, with 1 gm of catalyst in 100 ml of dilute aqueous solution, the minimum stirring speed required for complete catalyst suspension is 500 rpm; a stirring rate of 1000 rpm was therefore used in all experiments to ensure all catalyst was suspended.

The limiting reactant inside the catalyst particles is estimated by calculating the ratio of the observable modulus of hydrogen to that of alanine,[63] where the liquid-phase effective diffusivities of alanine and hydrogen are estimated using the Wilke-Chang equation.[64] For all reactions, the ratio of observable moduli was much greater than 1, indicating that hydrogen is the limiting reactant. Applying the Weisz-Prater[65] criterion to the observable modulus for hydrogen shows that the effect of mass transport inside the catalyst pores is negligible, as $\eta\varphi_{H_2}{}^2$ for H_2 is $<10^{-3}$ for all reaction conditions.

$$\frac{\eta\varphi_{H2}{}^2}{\eta\varphi_A{}^2} = \frac{1}{b}\frac{C_A D_{e,A}}{C_{H_2} D_{e,H_2}} \tag{1}$$

The Yagi and Yoshida[66] and Boon-Long[67] correlations were used to estimate gas-liquid (G-L) and solid-liquid (S-L) interfacial mass-transfer coefficients for H_2 and alanine, respectively. The maximum mass transfer rates, estimated as the product of the mass transfer coefficient and bulk liquid-phase concentration, were then calculated and found to be at least two orders of magnitude larger than the observed reaction rates, indicating

that the mass-transport resistances across phase boundaries were negligible under the experimental conditions studied.

In summary, from the analysis of various mass transfer processes we conclude mass transfer resistances do not limit amino acid conversions over the range of temperatures and pressures studied in this work.

3.4.4 Kinetic Model

In a prior publication,[24] we showed that alanine hydrogenation over ruthenium on carbon occurs by a two-site Langmuir-Hinshelwood (L-H) kinetic mechanism in which protonated amino acids adsorb on one type of surface catalytic site (S1) and hydrogen dissociatively adsorbs on a second type of site (S2). The final rate equation is given in Eq. (2) below. This two-site catalyst-substrate interaction is supported by the molecular modeling results of Neurock and coworkers[68] for hydrogenation of acetic acid over palladium. They show that the adsorbed acid is initially bound via the carboxylate ~2 Å above catalyst surface palladium atoms while the dissociated hydrogen atoms[69] nestle in the 3-fold coordinated interstices between surface metal atoms.

We have fit alanine hydrogenation data, presented in Figure 3 and determined at additional combinations of reaction conditions, to our previously developed kinetic model[24] given in Eq. (2).

$$-r_A = k_s \frac{K_A C_A^+}{(1 + K_A C_A^+ + K_P C_P)} \frac{K_{H_2} C_{H_2}}{\left(1 + \sqrt{K_{H_2} C_{H_2}}\right)^2} \qquad (2)$$

45

The model was applied with constants from the prior work,[24] except that the preexponential factor of the forward rate constant (k_s) in the model was adjusted downward by 40% from the original value[24] to represent the somewhat lower intrinsic activity of the particular lot of Ru catalyst used in this study. Equation (2) describes the current alanine hydrogenation data with <15% average error, a level of error similar to that found in our prior study.

Although Eq. (2) involving protonated alanine describes the data well, it is somewhat cumbersome to implement because the protonated alanine concentration must be calculated at each value of bulk concentration via a rather complicated charge balance involving alanine and phosphoric acid in all of their ionic forms. For multiple amino acid substrates, this charge balance is further complicated by multiple species and thus constitutes a significant barrier to the practical application of the model. Therefore, we have chosen here to develop an alternate model for amino acid hydrogenation involving total amino acid concentration. This simplified model is more amenable to mixed substrates and is still a valid description of hydrogenation, because for the rather narrow range of reaction conditions investigated here the fraction of total amino acid in protonated form only ranges from about 40% to 60% over the course of reaction. Thus, protonated acid concentration is for the most part proportional to the total amino acid concentration, and a viable, practical model can therefore be implemented.

The two-site Langmuir-Hinshelwood model, in which molecular hydrogen and amino acid adsorb on the catalyst surface and subsequently react to form amino alcohols, can be represented as follows.

$$A + S_1 \underset{K_A}{\overset{}{\rightleftharpoons}} A.S_1 \qquad (3a)$$

$$B + S_1 \underset{K_B}{\overset{}{\rightleftharpoons}} B.S_1 \qquad \Big\} \quad fast \qquad (3b)$$

$$H_2 + 2 S_2 \underset{K_{H_2}}{\overset{}{\rightleftharpoons}} 2 H.S_2 \qquad (3c)$$

$$A.S_1 + 2 H.S_2 \xrightarrow{k_S} A^*.S_1 + 2 S_2 \qquad slow \qquad (3d)$$

$$A^*.S_1 + 2 H.S_2 \rightleftharpoons Aol.S_1 + 2 S_2 \qquad fast \qquad (3e)$$

$$B.S_1 + 2 H.S_2 \xrightarrow{k_S} B^*.S_1 + 2 S_2 \qquad slow \qquad (3f)$$

$$B^*.S_1 + 2 H.S_2 \rightleftharpoons Bol.S_1 + 2 S_2 \qquad fast \qquad (3g)$$

$$Bol.S_1 \rightleftharpoons Bol + S_1 \qquad fast \qquad (3h)$$

$$Aol.S_1 \rightleftharpoons Aol + S_1 \qquad fast \qquad (3i)$$
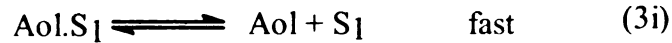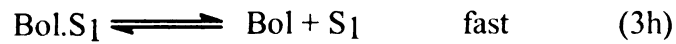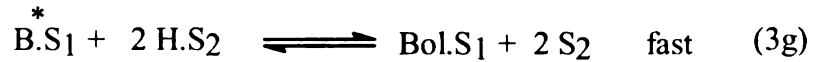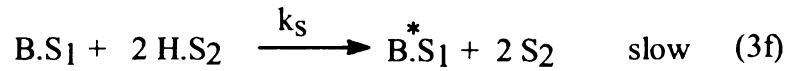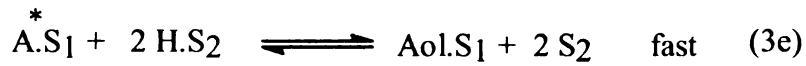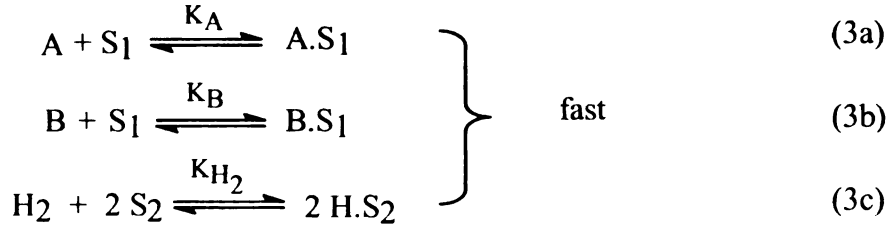
where A and B are the amino acids adsorbing onto active sites of type S1, A*S1 and B*S1 are adsorbed intermediates, and Aol and Bol are the amino alcohol products.

Derivation of the kinetic rate equation from the above mechanism follows the standard procedure for L-H kinetics, and results in the same form as Eq. (2) except with total amino acid concentration instead of the protonated species. In addition, in this work all reactions were run at 7.0 MPa, so the hydrogen pressure term is incorporated into the composite rate constant k'.

$$k' = k_s \frac{K_{H_2} C_{H_2}}{\left(1 + \sqrt{K_{H_2} C_{H_2}}\right)^2} \qquad (4)$$

The rate form for hydrogenation of a single amino acid therefore reduces to:

$$-r_A = \frac{k'_A K_A C_A}{(1 + K_A C_A + K_P C_P)} \qquad (5)$$

For the case of two amino acids A and B, the rate form is

$$-r_A = \frac{k'_A K_A C_A}{(1 + K_A C_A + K_B C_B + K_P C_P)} \qquad (6)$$

Values of the three composite reaction rate constants, k'_{serine}, $k'_{alanine}$, and

k'_{valine}, and the adsorption constants K_{serine}, $K_{alanine}$, K_{valine} and $K_{H_3PO_4}$ in the kinetic

model were determined by first estimating values for the constants and then numerically

integrating the rate expressions to obtain predicted concentration versus time profiles for

each reaction. Optimum rate constant values were then determined by varying the rate

constants systematically to minimize the error defined in Eq. (7) below.

$$\text{Error (\%)} = \frac{\displaystyle\sum_{n\,samples} \left| \dfrac{C_{A,pred} - C_{A,exp}}{C_{A,exp}} \right|}{n_{samples}} \times 100\,\% \qquad (7)$$

The error minimization was carried out over the entire dataset containing both individual and mixed amino acid hydrogenations. The resulting optimized rate constants are listed in Table 4.

Table 4. Kinetic constants for amino acid hydrogenation at 403 K.

Compound	Surface reaction rate constant $k_i\,'$ (kmol/(kgcat.hr))	Adsorption coefficient K_i (M^{-1})
Serine	0.018	56
Alanine	0.016	24
Valine	0.0015	124
H_3PO_4		19

Parity plots of experimental vs. predicted concentrations for each amino acids over all experiments gave correlation coefficients (R^2 values) of 0.98 for serine, 0.97 for alanine, and 0.99 for valine. The model prediction of amino acid concentration vs. time in reaction is given as lines in Figures 14, 17, and 18. For the optimized rate constants, the calculated average error between experimental and predicted amino acid concentrations was 14% for amino acid conversions up to 60%, and 38% for amino acid conversions up to 90%. Calculating error on a percentage basis as in Eq. (7) magnifies differences at low concentration, and since there is more uncertainty present in data at low concentrations because of handling and analytical uncertainties, the significantly higher error at high conversions is not unexpected. Fortunately, the model's uncertainty at low

49

concentrations, although high on a percentage basis, is small on the absolute concentration scale. Thus, the model predicts single and mixed amino acid hydrogenation data reasonably well over the full range of conditions examined.

The L-H rate expression provides insight into the relative surface concentrations of hydrogen and amino acid on the catalyst, as according to the L-H model the denominator terms (Eq. 5) give the relative concentrations of vacant, hydrogen-occupied, and amino acid-occupied surface sites. For example, at 0.22 M alanine concentration with 0.3 M H_3PO_4, alanine occupies 39% of the active sites, 52% of the active sites are occupied by phosphoric acid, and 9% of the active sites are unoccupied. If a second amino acid (serine) is added at a concentration of 0.22 M and the H_3PO_4 concentration is increased to 0.5 M, the distribution of site occupation is 15% alanine, 46% serine, 35% H_3PO_4, and 4% unoccupied. Thus, the second amino acid reduces the number of active sites occupied by the original amino acid, resulting in a decrease in conversion rate for the latter.

The adsorption affinity of the amino acids on the catalyst, as reflected in the values of adsorption constants in Table 4, is valine > serine > alanine. The strong adsorption of valine is evidenced by its essentially zero order behavior at higher concentrations. The reason why valine adsorbs more strongly is not fully understood, but valine is a larger molecule and more "organic" in character, so it may prefer to adsorb on the surface as opposed to remaining in the aqueous phase. Further study will be required to understand fully the adsorption affinities of the different amino acids.

3.5 Conclusions

The hydrogenation of serine, alanine and valine and their mixtures in aqueous solutions has been examined. The presence of more than one substrate affects hydrogenation rates through competitive adsorption. Of the three amino acids, serine and alanine exhibit comparable reactivity, while valine is hydrogenated at a considerably slower rate. A Langmuir-Hinshelwood kinetic model with surface reaction as the rate limiting step describes the behavior of both single and mixed amino acid hydrogenation using a single set of parameter values. Valine has the largest adsorption constant, suggesting that strong valine adsorption is responsible for valine excluding other amino acids from active sites and for the observed zero-order valine behavior, both leading to reduced reactivities.

Acknowledgements

Nomenclature

Species

A = amino acid A

$A \cdot S_1$ = adsorbed amino acid A

$A^{*}{\cdot}S_1$ = adsorbed intermediate

Aol = amino alcohol from amino acid A

$Aol{\cdot}S_1$ = adsorbed amino alcohol from amino acid A

B = amino acid B

$B{\cdot}S_1$ = adsorbed amino acid B

$B^{*}{\cdot}S_1$ = adsorbed intermediate

Bol = amino alcohol from amino acid B

$Bol{\cdot}S_1$ = adsorbed amino alcohol from amino acid B

H_2 = molecular hydrogen

$H{\cdot}S_2$ = adsorbed hydrogen

P = phosphoric acid

S_1 = amino acid hydrogenation site

S_2 = hydrogen adsorption site

Variables

$\eta\varphi_j{}^2$ = observable modulus for species j

b = stoiciometric ratio of hydrogen to amino acid

C_j = concentration of species j, $kmol/m^3$

k'_j = surface reaction rate constant for species j, k_S / K_A, $kmol/kgcat{\cdot}s$

k_S = surface reaction rate constant, $kg_{cat}{}^2/kmol^2{\cdot}s$

K_A = adsorption coefficient of protonated amino acid A, $m^3/kmol$

K_B = adsorption coefficient of protonated amino acid B, $m^3/kmol$

K_P = phosphoric acid adsorption coefficient, $m^3/kmol$

K_{H_2} = adsorption coefficient of phosphoric acid $m^3/kmol$

$-r_A$ = reaction (consumption) rate of amino acid A, $kmol/kgcat{\cdot}s$

$D_{e,j}$ = effective diffusivity of species j, m^2/s

References

22 Jere, F. Catalytic Hydrogenation of Amino Acids and Polyhydroxyalkanoates. Ph.D. Dissertation, Michigan State University, East Lansing, MI, 2003.

23 Molengraft, A. Catalytic hydrogenation of 2,5-piperazinedione to piperazine. M.S. Thesis, Michigan State University, East Lansing, MI, 2006.

24 Jere, F.; Jackson, J.; Miller, D. Kinetics of the Aqueous-Phase Hydrogenation of L-Alanine to L-Alaninol. *Ind. Eng. Chem. Res.* **2004**, *43*, 3297.

25 Jere, F.; Miller, D.; Jackson, J.. Stereoretentive C-H Bond Activation in the Aqueous Phase Catalytic Hydrogenation of Amino Acids to Amino Alcohols. *Org. Lett.* **2003**, *5(4)*, 527.

26 Antons, S.; Beitzke, B. Process for preparing optically active amino alcohols. U.S. Patent 5,536,879, 1996.

27 Antons, S.; Tilling , A.; Wolters E. Method for producing optically active amino alcohols. U.S. Patent 6,310,254, 2001.

28 Schrauth W., . Schenck O, and Stickdorn K., *Ber.*, **1931**, 64, 1314

29 Guver A., Bieler.A. and Jabere. K., *Helv. Chim.Acta,,* **1947**, 30, 39; Sandoz'Ltd., German Patent 711,180,Aug. 21, 1941 [Chem. Abstr., 1940, 37, 3767]

30 Schuckmann G., U. S. Patent 2,332,834, Oct. 26,1944; Bohme-Fellchemie-Ges.m.b.H., French Patent 819,255,Oct. 13, 1937 [Chem. Abstr., 1938, 32, 2143]

31 Schmidt O., U. S. Patents 2,322,095-9, June 15, 1943; Schiller G., U. S. Patents 2,121,367-8, June 21, 1938.

32 Arnold H. R. and Lazier W. A., U. S. Patent 2,116,552, May 10, 1938.

33 Ford T. A., U. S. Patent 2,607,807, Aug. 19, 1952; Carnahan J. E., Ford T. A., Gresham W. A., Grigsby W. E., and Hager G. F., J. Org. Chem., 1955, 77, 3766.

34 Broadbent H. S., Graham C. C., Bartley W. J., and Johnson J. H., *J. Org. Chem.*, **1959**, 24, 1847.

35 Lazier W. A., U. S. Patent 2079414, 1937

36 Christiansen J. A., U.S. Patent 1302011, 1919

37 Evans J. W., Casey P. S., Vainwright M. S., Trimm D. L., Cant N., *Appl. Catal. A: General* **1983**, 7, 31-41

38 Sorum P.A., Onsanger O.T., *Proc. Int. Congr. Catal.*, **1984**, 8, 233-244

39 Monti D. M., Cant N. W., Trimm D. L. and Mainwright M. S., *J. Catal.*, **1986**, 100, 17-27

40 Evans J.W., Mainwright M. S., Cant N. W. and Trimm D. L., *J. Catal.* **1984**, 88, 203-213

41 Claus P., Lucas M., Lucke B., *Appl. Catal. A: General*, **1991**, 79, 1-18

42 Yan T. Y., Albright L. F., Case L. C., *Ind. Eng. Chem. Res. Prod. Res. Dev.* **1965**, 4, 101-110

43 Turek T., Trimm D. L., Cant N. W., *Catal. Rev. Sci. Eng.*, **1994**, 36, 645

44 Adkins H., Billica H. R., *J. Am. Chem. Soc.*, **1948**, 70, 3121-3125

45 Mozingo and Folkers, *J. Am. Chem. Soc.*, **1948**, 70, 227

46 Mozingo and Folkers, *J. Am. Chem. Soc.*, **1948**, 70, 229.

47 Adkins H., Billica H. R., *J. Am. Chem. Soc.*, **1948**, 70, 695-698

48 Thomas D. J., Vehrli J. T., Mainwright M. S., Trimm D. L *Appl. Catal A: General* **1992**, 86, 101-114.

49 Turek T., Trimm D. L,. Black D. S., Cant. N. V., *Appl. Catal A; General* **1994**. 116. 137-150.

50 Segel E., *J. Am. Chem. Soc.*, **1952**, 74, 1096

51 Studer M., Bruckhardt S., Blaser HU., *Adv. Synth. Catal.*, **2001**, No.8, 343,

52 Varga N., M. S. Thesis, Department of Chemistry, Michigan State University, 2002

53 Zhang Z. G., Jackson J.E., and Miller D. J., *Appl. Catal. A-Gen.*, **2001**, 219, 89.

54 Antons S., U.S. patent 5,536,879

55 Antons S., Tilling A., Wolters E., WO9938838, 1999.

56 Jere F., Jackson J. E., Miller D. J., *Ind. Eng. Chem. Res*, **2004**, 43, 3297.

57 Jere F., Miller D. J., Jackson J. E., *Org. Lett.* **2003**, 5(4), 527.

58 Chen Y., Miller D. J., Jackson J. E., *Ind. Eng. Chem. Res*, **2007**,46, 3334.

59 Lahr D. G., Shanks B. H., *Ind. Eng. Chem. Res.* **2003**, 42, 5467-5472

60 Dunn, M. S.; Ross, F. J.; Read L. S. The Solubility of the Amino Acids in Water. *J. Biol., Chem.* **1933**, *103 (2)*, 579.

61 Dalton, J. B.; Schmidt, C. L. A. The solubilities of certain amino acids and related compounds in water, the densities of their solutions at twenty-five degrees, and the

calculated heats of solutions and partial molal volumes. II, *J. Biol., Chem.* **1935**, *109 (1)*, 241.

62 Zwietering, T. N. Suspending of solids in liquid by agitators, *Chem. Eng. Sci.* **1958**, *8*, 244-253.

63 Ramachandran, P.; Chaudhari, R; *Three-Phase Catalytic Reactors*; Gordon and Breach Science Publishers: Philadelphia, PA, 1983.

64 Wilke, C.; Chang, P. Correlation of diffusion coefficients in dilute solution. *AIChE J.* **1955**, *1*, 264-270.

65 Weisz, P.B.; Prater, C. D. Interpretation of measurements in experimental catalysis. *Adv. Catal.* **1954**, *6*, 143-196.

66 Yagi, H.; Yoshida, F. Gas absorption by Newtonian and non-Newtonian fluids in sparged agitated vessels. *Ind. Eng. Chem. Process Des. Dev.* **1975**, *14 (4)*, 488-493.

67 Boon-Long, S.; Laguerie, C.; Couderc, J. Mass transfer from suspended solids to a liquid in agitated vessels. *Chem. Eng. Sci.* **1978**, *33 (7)*, 813-819.

68 Pallassana, V.; Neurock, M. Reaction paths in the hydrogenolysis of acetic acid to ethanol over Pd(111), Re(0001), and PdRe alloys. *J. Catal.* **2002**, *209 (2)*, 289-305.

69 Singh, U. K.; Vannice, M. A. Kinetics of liquid phase hydrogenation reactions over supported metal catalysts A review. *Appl. Catal., A: Gen.*, **2001**, *213 (1)*, 1.

Chapter 4. PDMS-glass Microreactor

4.1 Introduction

Work presented in the following sections arose from the need to address the following problems and related opportunities:

- Aqueous phase catalytic hydrogenations involve considerable gas liquid mass transfer resistance. This, coupled with low solubilities of hydrogen in the reaction mixture (0.02 M at 350 psi and 27 °C; 0.056 M at 1050 psi and 27 °C), results in the need for high pressures and mechanical stirring to ensure availability of hydrogen at the active site of the catalyst. In spite of this, a large number of heterogenous hydrogenations involve hydrogen as the limiting reactant. Microchannel reactors, on the other hand, present a very small cross sectional path length and hence very low resistance to the diffusion of hydrogen to the active site. Thus, high pressure hydrogenations, if carried out in a microchannel reactor with immobilized catalyst, would result in conditions where hydrogen is not the limiting reactant. This would allow study of the intrinsic kinetics of aqueous phase hydrogenation, which is otherwise difficult to examine.

- Nanoparticulate catalysts are unstable and tend to agglomerate over long durations. This tendency to agglomerate can be aggravated by high temperatures and other conditions commonly found in heterogeneous catalytic reactions. One strategy to study nanoparticle behaviour as catalysts, while preventing agglomeration, is to anchor the nanoparticles on porous supports. Another strategy can be to pass reaction mixture over a monolayer of catalytic nanoparticles – this would allow characterization of the activity of nanoparticles towards hydrogenation in the absence of any interactions by the support.

57

To implement the above approaches, a microchannel reactor would have to be immersed in a hydrogen rich environment. One face of the microchannels could be a catalytic membrane permeable to hydrogen, such as a palladium membrane. The hydrogen could thus diffuse through the membrane into the microchannels, while the palladium simultaneously catalyzes the reaction. The lack of mechanical stability of most microchannel reactors to pressure differentials (between inside and outside of the microreactor) greater than 50 psi is an inherent limitation of such an approach. A different solution would involve presaturating the reaction mixture passing through the microchannels with hydrogen gas at high pressure, thus allowing equal pressures inside and outside the microreactor and eliminating pressure gradients and related problems of mechanical integrity. It is this latter approach which is presented in the following sections.

4.2 Immobilization of Catalytic Nanoparticles

Exploratory work in the Miller Jackson lab (Dr. Kausik Mukhopadhyay) demonstrated that ruthenium nanoparticles supported on MCM-41 were active towards the catalytic reduction of lactic acid and glycine[70], as shown in Table 5 below. On a per mole ruthenium basis, the nanocatalysts exhibit an order of magnitude increase in catalytic activity towards hydrogenation as compared to carbon-supported ruthenium catalysts.

Table 5. Results of Lactic acid hydrogenation using various supported nanocatalysts, courtesy Dr. Mukhopadhyay (PG= propylene glycol, Ru = ruthenium, APTS = amino propyl trimethyl silane, Y = zeolite Y, M41 = MCM 41, Ru/C = ruthenium supported on carbon)

Catalysts	Temp. (K)	Press. (MPa)	Substrate 0.1(M)/ mL	Speed (rpm)	Time (hours)	Conv. (%)	Selectivity (%)	Catalyst (g)
Ru-APTS-Y	403	6.9	50	1000	48	10	52 (PG)	0.10
Ru-APTS-Y	403	6.9	50	1000	48	11	52 (PG)	0.10
Ru-APTS-M41	403	6.9	50	1000	48	30	98.5 (PG)	0.10
Ru-M41-1	403	6.9	50	1000	24	32	99.3 (PG)	0.10
Ru/C	403	6.9	50	1000	48	51.5	99.2(PG)	0.50

However, to understand the behaviour of nanocatalysts, it is important to characterize their activity in the absence of interactions with the support, and to immobilize them in an appropriate manner. Work by Kobayashi et al.[71] has shown that hydrogenation catalysts can be immobilized onto the glass surface of a microchannel reactor. They achieved this by functionalizing the silica groups on the glass surface using an amine, and cross linking microencapsulated palladium onto the functionalized glass surface. A few workers have coated glass with titania-palladium[72]. Based on prevalent literature, it was decided to pursue a strategy based on coating the glass face with titania and then immobilizing ruthenium nanoparticles onto the coated glass. Once a monolayer of catalyst had been immobilized onto the glass surface of the microreactor, the microreactor would be placed in a high pressure reactor to enable liquid saturated with hydrogen gas at high pressures to flow past the catalyst.

4.3 PDMS-Glass Microreactors

PDMS (Poly DiMethyl Siloxane) based microreactors are usually formed by soft lithography[73]. This technique starts by spin coating a layer of photoresist up to 200μm thick onto a support. This photoresist is then exposed to UV light through a pattern printed on a transparency. The photoresist cures on exposure to UV light. The rest of the photoresist can be dissolved away, leaving a mould which can be used to cast multiple PDMS microchannels. The PDMS prepolymer is poured onto the mould and cured at 70 °C for 2 hours. On hardening, the PDMS microchannels slab is ready to be plasma bonded to glass to form a PDMS glass microreactor (Figures 21,22 and 23).
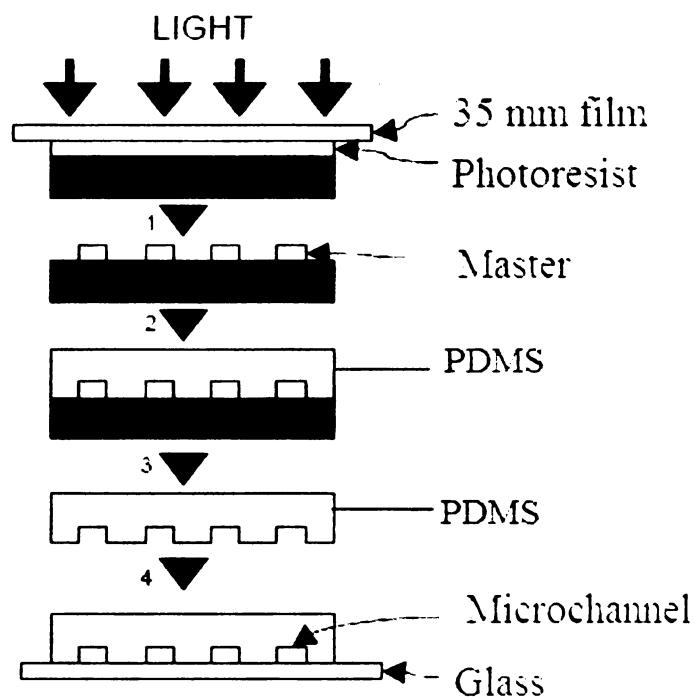
Figure 21. (1) photolithography is preformed to produce the master, (2) the PDMS positive is created using the master, (3) remove the polymerized PDMS from the master, (4) seal the PDMS against a glass cover slide using plasma bonding to create the microchannels. Figure taken from reference 74.

60

4.4 Design of System - Modeling and Preliminary Calculations

To determine feasibility, the proposed system was modeled as a differential batch reactor, i.e. essentially a 10 ml batch reactor with a certain amount of catalyst loading. Preliminary calculations for catalyst loading were as follows:
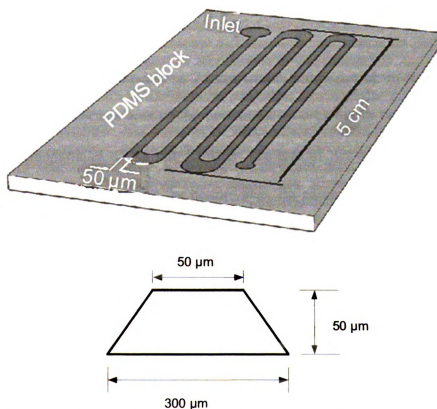
Figure 22. Schematic showing a) dimensions of microchannels engraved in a block of PDMS using soft lithography. b) Cross section of a PDMS microchannel.
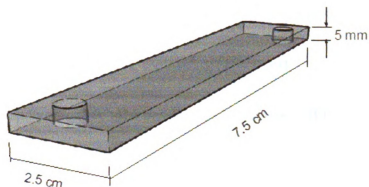
Figure 23. Dimensions of a glass slide with holes, which is plasma bonded to PDMS block engraved with microchannels to form a PDMS glass microreactor. (Schematics not to scale).

For microreactor dimensions 25 cm length × 600 μm channel width × 50 μm channel depth, the surface area of the bottom face works out to be 1.5×10^{-4} m^2. For ruthenium nanoparticles of 3.5 nm diameter, this area allows approximately 1.1×10^{13} nanoparticles as a monolayer on the bottom face. Based on a ruthenium bulk density of 12.03 gm/cm^3, 4 micrograms of the ruthenium nanoparticles could thus be incorporated as a monolayer of nanoparticles onto the bottom face of the microreactor.

For 3 micrograms of Ru nanoparticles (of diameter 3.5 nm), the total surface area is 4.2×10^{-4} m^2. Hydrogenation of alanine was chosen as a model reaction, the reaction rate based on active surface area of catalyst being 0.004 mol/(m^{2}Ru·hr), for Ru/C catalyst, as seen from an experimental study of hydrogenation of amino acid mixtures and confirmed from previous work by Frank Jere in our laboratory[24]. For such a reactor with the above assumptions,

$$V\frac{dC_A}{dt} = r_A \times A_{cat}$$

where V = volume of the reactor, liters $= 1 \times 10^{-2}$

C_{AO} = concentration of substrate amino acid A, mol/lit = 0.005

$-r_A$ = reaction rate for substrate A, mol/(m²cat·hr) = 0.004

A_{cat} = total catalyst surface area possible on bottom face of microchannel with a monolayer of 3.5 nm particles, $m^2 = 4 \times 10^{-4}$

Using these values, $dC_A/dt = 1.83 \times 10^{-4}$ mol/(lit·hr) and $dX_A/dt = 0.04$ hr^{-1}. Thus, the system would give 4% conversion of the starting material per hour. Given a method to immobilize catalyst on the bottom face of the microchannel, the required catalyst loading could be achieved, and thus, the proposed system appears to be feasible.

4.5 Design of System – Flow Loop and System Constraints

The proposal divided the goal into two major sub tasks, viz. to establish a reactor configuration and demonstrate test reaction within the assembled setup.

1) Establish reactor configuration

High hydrogen pressures are necessary for hydrogenation but the PDMS microchannel reactor being used could only withstand pressures of up to 0.5 MPa. Hence, a novel reactor configuration involving equally high hydrogen pressures both within and outside the microreactor was proposed. This involved placing a microreactor in a high pressure Parr reactor, with pressure in the Parr reactor adjusted so that there was equal hydrogen pressure both within and outside the microreactor, as shown in Figure 24.
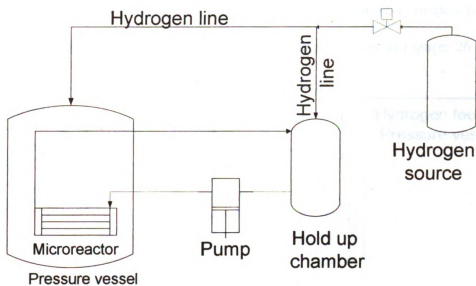
Figure 24. Schematic of proposed microreactor-in-pressure-vessel setup

2) Test reactions

The PDMS microreactor swells in organic solvents, and has limited temperature stability[75] (373 K). Hence, test reactions should ideally be low temperature and low hydrogen pressure, such as hydrogenation of acetone.

4.6 Development of the Flow Loop

During the development of the microreactor setup, changes were made to the design. It was decided that the holdup reservoir could be incorporated within the Parr reactor itself. Initially, the holdup volume at the bottom of the Parr reactor was chosen as the reservoir. Further modifications were made by inserting a 7-ml vial placed in the Parr reactor was used as a reservoir (Figure 25). This reduced the length of the flow loop,

enabled better control over temperature and pressure in the various components of the setup, and reduced the volume of the reservoir. The setup is shown in Figures 26 and 27.
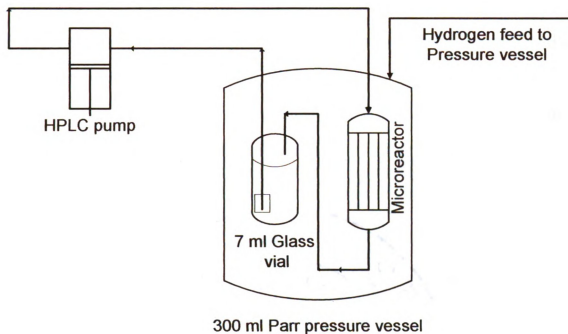
Figure 25. Schematic of modified flow loop
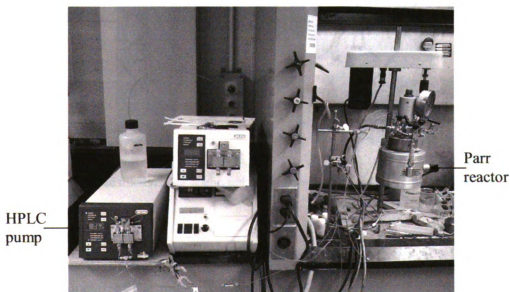
Figure 26. Various components of the flow loop

All tubing connections were made using standard 1/16" O.D. HPLC tubing (initially steel, later replaced by polymeric tubing). One sixteenth inch S.S. 316 steel ferrules were used to seal the tubing as it entered and left the high pressure Parr reactor. The vial was open to the contents of the Parr reactor, thus by pressurizing the Parr reactor, the contents of the vial and associated tubing were also pressurized. This ensured that the pressures within the microreactor and that outside the microreactor were equal.
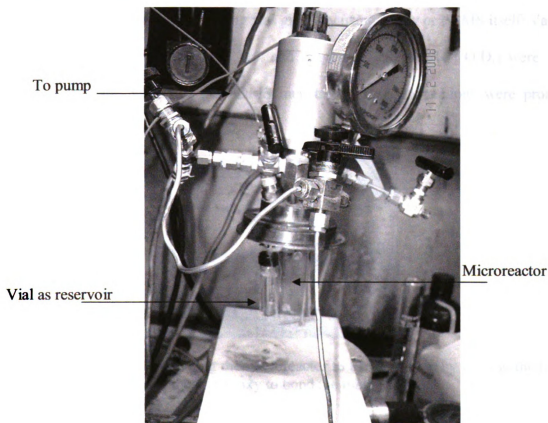
Figure 27. Close up of the microreactor connected to the flow loop and located inside the Parr reactor

4.7 Flow Loop: Connections between the Microreactor and the HPLC Tubing

The diameter of the microchannels in the PDMS-glass microreactor was of the order of 50 μm. This is considerably smaller than the diameter of standard HPLC tubing. Also, the flow through the microchannels is likely to result in a pressure drop of the order

of 0.1 to 0.2 MPa. Hence, to prevent leakage, connections at the inlet and the outlet of the microreactor needed to be mechanically strong. There is a considerable amount of literature dealing with connections between the micro and macro parts of a microchannel system[76], but the high pressures involved in the current setup, especially at startup, led us to develop alternatives. We began by passing the HPLC tubing through the PDMS block of the PDMS-glass microreactor (Figure 28), such that the tubing would be open to the ends of the microchannels. The tubing was glued by using epoxy or PDMS itself. Various types of tubing (polyethylene, S.S.316, and polyimide, all of 1/16" O.D.) were tried. However, the soft nature of the PDMS meant that these connections were prone to leakage once flow was started.
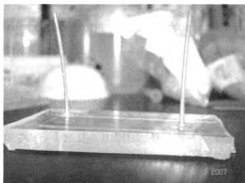
Figure 28. Attempt at connecting the microreactor to the flow loop by passing the tubing through the PDMS side and using epoxy to bond the tubing in place.

The next approach therefore relied on passing the tubing through the glass side of the PDMS-glass microreactor. Holes were drilled or sand blasted into the glass before plasma bonding. The holes through thin glass slides (thickness 1 mm) afforded too little surface area for epoxy binding to the tubing. Consequently, glass slides with a thickness of 10 mm were tried (Figure 29). With these slides, a strong and leak proof connection could be obtained between the inlet / outlet tubing and the microreactor. However, the

uneven nature of their surface resulted in an uneven plasma bond between the glass and the PDMS, leading to leakage at the PDMS-glass interface. Slides with a thickness of 5 mm were better suited to the task at hand and were used in further studies.

Figure 29. Tubing connections to the microreactor through a 10 mm glass slide.

Other alternatives tested included slides with 1 mm thickness having glass tubes glued onto them to act as ports for the tubing, but the ports themselves would come apart after 36 hours.

4.8 Catalyst Immobilization

Initially tests were performed to ensure that the setup was leak proof. Various approaches towards immobilization of nanoparticles were being tried out. These included using APTS (Amino Propyl Trimethyl Silane) as an anchoring agent between the glass and the ruthenium nanoparticles, and using biotinylated palladium to enhance bonding to the glass slide. Immobilization of bulk metals such as palladium or platinum within the microchannels was suggested as a practical and elementary approach for demonstrating

reactivity within the proposed setup. Although this approach would give catalytic surface area two orders of magnitude smaller than the immobilized nanoparticles originally planned, it would nevertheless validate the concept. Hence, palladium microwires of 50 micron diameter were placed in the microchannels before irreversible bonding to the glass, as shown in Figure 30.
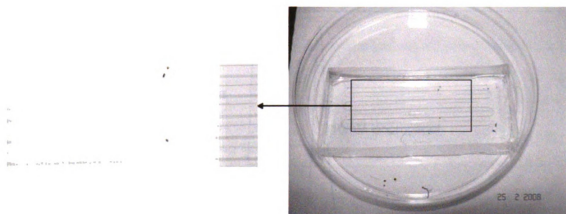
Figure 30. Pd wires placed inside the microchannels in a PDMS block.

4.9 Choice of Substrate

The substrate chosen had to be reactive enough to demonstrate significant conversion to the hydrogenation product at low temperatures, viz. 50 deg C. Hydrogenation of acetone to isopropanol proceeds relatively fast under such mild reaction conditions. Additionally, the existing analytical setup was capable of analyzing acetone and isopropanol at the low concentrations being considered. Hence hydrogenation of acetone was selected as a test reaction. A schematic of the reaction is shown in Figure 31 and a chromatogram is shown in Figure 32.
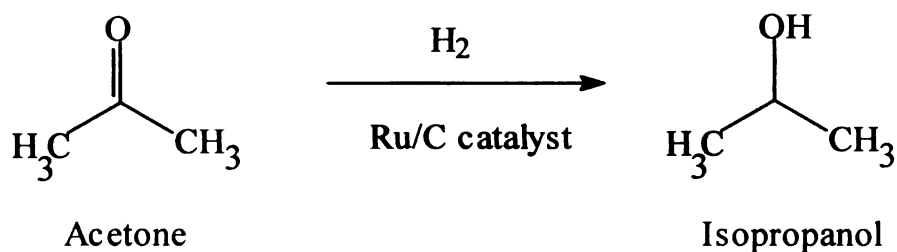
Figure 31. Hydrogenation of acetone to isopropanol. Standard reaction conditions: 323K temperature and 700 psi hydrogen,
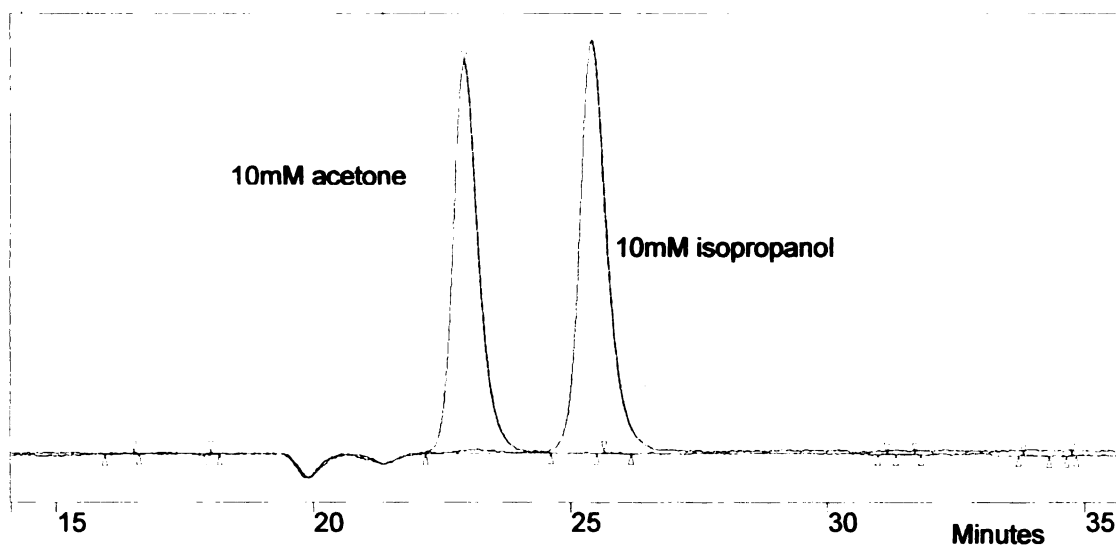
Figure 32. Chromatogram showing RI response and elution times of acetone (23 min) and isopropanol (25.5 min). 5 mM H_2SO_4 as mobile phase, 0.6 ml/min, 60 °C, Aminex column (Bio-Rad HPX-87H ion exclusion column)

4.10 Results and Discussion

Five ml of 5mM acetone in water was subjected to hydrogenation in the microreactor setup. A typical run involved passing the reaction mixture at 1 ml/min through the flow loop for 20 hours. The temperature of the system was varied between 22 and 55 °C between runs, while hydrogen pressure was kept constant at 350 psi or higher. Five mM glycerol was used as an internal standard on account of its negligible volatility under reaction conditions. This in conjunction with control runs without any catalyst gave

70

an estimate of the amount of acetone lost due to evaporation during each run. Table 6 summarizes results from the runs.

Table 6. Summary of results from hydrogenation runs using Pd wire immobilized in PDMS-glass microreactor

Feed	reaction conditions	Catalyst	Yield to IPA +/- 4%
5 ml of 6mM acetone + internal standard	20 °C, 350 psi H_2, 22 h at 1 ml/min	25 cm of 50 µm Pd wire	3.5 %
5 ml of 6mM acetone + internal standard	22 °C, 350 psi H_2, 22 h at 1 ml/min	**no catalyst**	0.75 %
5.5 ml of 8.8 mM acetone + internal std.	**55 °C, 725 psi H_2** 22 h at 1 ml/min	25 cm of 50 µm Pd wire	6 %
5.5 ml of 8.8 mM acetone + internal std.	55 °C, 725 psi H_2 **92 h** at 1 ml/min	25 cm of 50 µm Pd wire	36 %
5.5 ml of 8.8 mM acetone + internal std.	55 °C, **no H_2** 21.5 h at 1 ml/min	25 cm of 50 µm Pd wire	No IPA observed

To compare the reactivity seen with Pd wire with that seen in the case of Ru/C catalysts, a calculation for the Turn Over Frequency (TOF) was performed as follows:

From amino acid studies, 100 ml of 0.22 M alanine solution reacts completely in 5 hours. Hence 0.022 moles of amino acid react in 5 hours.
Catalyst used was 1 gm of 5 % Ru/C, i.e. 0.05 gm or Ru. With a metal dispersion of 10%, the active metal weight is 0.005 gm or 5×10^{-5} moles.
Thus the turnover frequency for amino acid hydrogenation

$$TOF\left(\frac{\text{mol alanine}}{\text{mol Ru}\times\text{sec}}\right) = \frac{0.022\,mol.alanine}{5hr}\times\frac{1}{5\times10^{-5}\,moles.Ru}\times\frac{1hr}{3600s} = 0.02$$

In the case of the Pd wire in the microreactor, the calculations are as follows:
Number of moles of acetone reacted: 8.4×10^{-7} moles in 22 hours.
Surface area of 25 cm of 50 μm Pd wire is 8×10^{-6} m^2
Radius of a palladium atom is 1.69×10^{-10} m
Cross sectional area of a Palladium atom is 8.97×10^{-20} m^2
No of atoms in area 8.7×10^{13}
No of moles of Pd on surface of Pd wire is 1.5×10^{-10} moles
Thus the turnover frequency for acetone hydrogenation is 0.07 moles acetone/mole Pd/s

$$TOF = \frac{8.4\times10^{-7}\,mol.acetone}{22hr}\times\frac{1}{1.5\times10^{-10}\,moles.Pd}\times\frac{1hr}{3600s} = 0.07$$

From the above calculations, it can be seen that the turn over frequencies are of the same order of magnitude in both cases, even though these are different catalyst metals.

It should be noted that the result obtained in the absence of any catalyst, line 2 in Table 6, shows that the hydrogenation of acetone to isopropanol can proceed, albeit to a small extent (1%), in the absence of any catalyst. One possible source of this reactivity can be the metal from the stainless steel tubing used in the flow loop. To minimize this possibility, all steel tubing was replaced by polymeric PEEK tubing. However, it was not possible to remove metal from the flow loop entirely since the pump heads and valves utilize stainless steel as primary material of construction. To confirm that the catalyst was indeed playing a significant role, it was decided to increase the catalyst loading.

4.11 Attempts at Increasing Catalyst Loading

To ensure that the conversion to IPA observed in the experiments was catalytic and not due to background reactivity alone, attempts were made to increase the catalyst

loading inside the microreactor. These included mixing Pd/C with the PDMS prepolymer to test if any Pd/C would be exposed in the surface of the microchannels. Both this approach and introduction of Pd precursors such as $PdCl_3$ into the PDMS before curing resulted in negligible amounts of Pd on the surface of the microchannels as measured by XPS.

4.12 Conclusion

A PDMS-glass microreactor was incorporated into a 300 ml high pressure hydrogenation reactor. A flow loop was developed which ensured equal pressure inside and outside the microreactor, overcoming limitations related to mechanical stability of the microreactor. As a result, liquid saturated with hydrogen at high pressures could be passed through the microchannels. This eliminates gas liquid mass transfer resistance, and enables the study of intrinsic reaction kinetics under conditions where hydrogen is not the limiting reactant. Preliminary results were obtained using immobilized palladium wires. However, increase in the catalyst loading or active catalytic surface area is necessary to demonstrate sufficient enhancement in reaction rates. This can be achieved by immobilizing nanoparticulate catalysts in the microchannels, an approach which is being pursued by our colleagues, or by developing a different immobilization technique altogether as demonstrated in Chapter 5.

References

70 Mukhopadhyay K., Jackson, J. E., Miller D. J., unpublished results.

71 Kobayashi J., Mori Y., Okamoto K., Akiyama R., Ueno M., Kitamori T., and Kobayashi S., *Science*, **28 May 2004**, *304*, 1305-1308.

72 Carturan, G.; Facchin, G.; Navazio, G.; Gottardi, V.; Cocco, G. Ultrastruct. Process. Ceram., Glasses, Compos., [Proc. Int. Conf.] (1984), Meeting Date 1983, 197-206 Publisher: Wiley, New York, N. Y, editors Hench, Larry L.; Ulrich, Donald R.

73 McDonald J., Whitesides G., *Accounts of Chemical Research*, vol 35, no 7, pg 491 (2002)

74 Zwolinski A. M., Ph. D. Thesis, The Florida State University College of Engineering, Spring 2004

75 Lee J. N., Park C., and Whitesides G., *Anal. Chem.*, vol 75, pp. 6544-6554 (2003)

76 Bhagat A. A. S., Jothimuthu P., Pais A., and Papautsky I., *J. Micromech. Microeng.*, 17, 42–49 (2007)

Chapter 5. PDMS Tubing as Microreactor

Because of the challenges encountered in immobilizing catalyst in and making secure plumbing connections to the PDMS-glass microreactor, it was decided to use PDMS tubing itself as the microreactor. This approach greatly reduced the time required in testing a prototype, since it eliminated the time lost due to leaking microreactors.

5.1 Development of Immobilization Technique

It was decided that slurry deposition was the most straightforward approach to immobilization of the catalyst in the PDMS microchannels. However, solvents such as water do not wet the surface of the microchannels and this did not result in any immobilization. A search through the literature revealed that there were very few solvents capable of interacting with the microchannel material on time scales fast enough to allow evaporative deposition. A screening of various solvents led us to amines as suitable solvents for the catalyst slurry. Additionally, catalyst, once deposited by the evaporating solvent front in the microchannels, was fairly strongly immobilized – repeated washes with solvents did not result in any significant leaching of the catalyst.

5.2 Immobilization Procedure

Silicone (essentially PDMS) tubing of 0.03 inch I.D., 0.065 inch O.D. was procured from VWR Scientific Products (Catalog number 60985-706). A piece of tubing of known length (ranging from 30 cm to 70 cm) was weighed. A slurry of 80 mg Ru/C catalyst in 5 ml diisopropylamine was drawn into the tubing, 1 ml at a time, such that at a time the slurry occupied not more than 5 cm of the tubing. The drawn slurry was allowed

to stand in the tubing for 1 minute to allow the solvent to evaporate. The evaporating solvent front deposited a layer of catalyst particles on the tubing walls. This procedure was repeated, with a different region of the tubing (of length 2 cm) being targeted for deposition each time, until most of the tubing had catalyst deposited in its interior. After all the solvent had evaporated, the tubing was weighed. Subsequently the tube was flushed with water to remove any undeposited catalyst. Drying and weighing again complete the procedure. The resultant catalyst loadings ranged from 3 to 8 mg of Ru/C deposited per foot of tubing (Figure 33).

After 50 hours in 10 runs we saw little or no leaching of the catalyst or decrease in catalytic activity. The above immobilization technique thus allows easy immobilization of a catalyst of choice in the microchannel tubular reactors that are cheap and readily available. It is thus potentially a significant contribution to the field of catalytic microreactor technology.
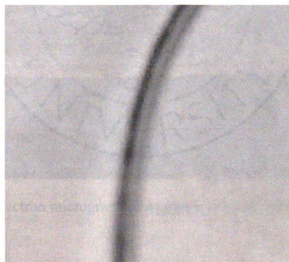
Figure 33. PDMS tubing with Ru/C catalyst deposited inside the tubing

Scanning Electron Micrographs of a cross section of the tubing showed Ru/C catalyst uniformly deposited along the length of the tubing. Catalyst particles ranged in size from 2 to 50 microns. From the SEM images (Figures 34 to 36), the retention of activity and the constant weight of the tubing after a number of experiments, it can be concluded that the catalyst is firmly anchored to the tubing.
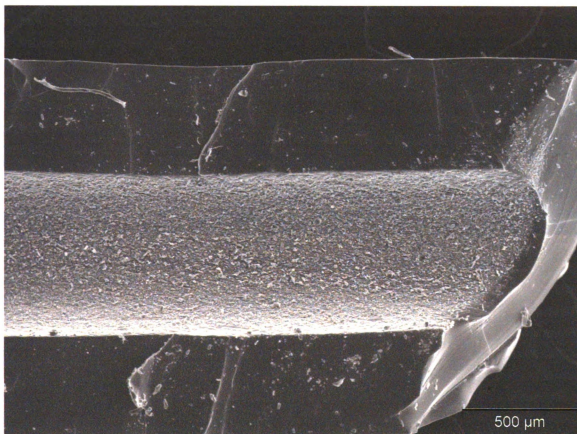
Figure 34. Scanning electron micrograph of a cross section of PDMS tubing with immobilized catalyst
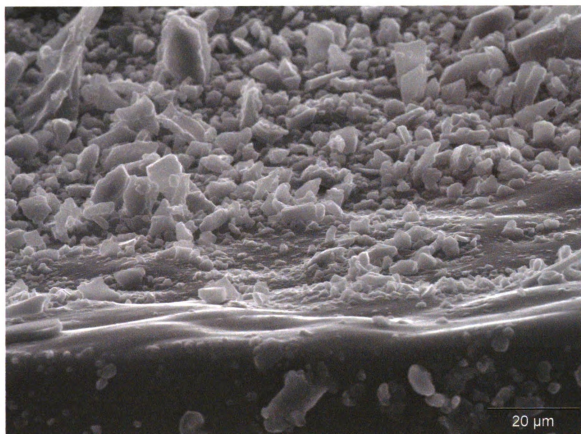
Figure 35a. Scanning electron micrograph of a cross section of PDMS tubing with immobilized catalyst
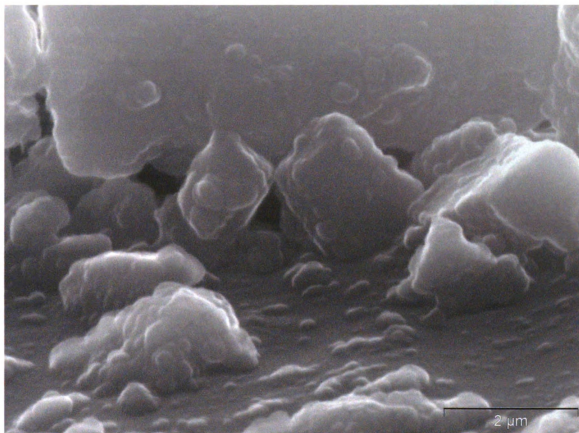
Figure 35b. Scanning electron micrograph of a cross section of PDMS tubing with **immobilized catalyst**
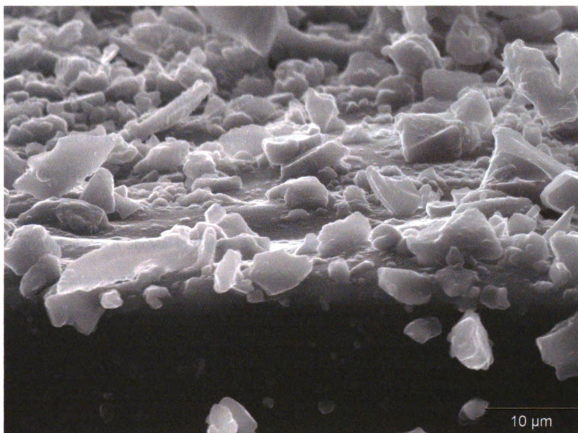
Figure 36. Scanning electron micrograph of a edge of a cross section of PDMS tubing with immobilized catalyst

5.3 Methods

Reactions were performed by connecting the catalytic tubing described above to the high pressure hydrogenation setup described in the earlier chapter. The catalytic tubing replaced the PDMS glass microreactor used in that setup. As before, 7.5 ml of the reaction mixture was recirculated through the reactor using an external HPLC pump at 0.25 ml/min for the time of reaction, generally 1 hour. Hydrogen pressure was maintained at 650 psi and the temperature was maintained at the desired level using the heater integral to the 300 ml Parr reactor.

Analysis of 200 μl samples drawn at regular intervals was performed using an HPLC setup equipped with refractive index (R.I.) detector. Data from the U.V. detector

was collected but not used. The column used was an Aminex column (Bio-Rad HPX-87H

ion exclusion column), maintained at 60°C in the HPLC oven. The mobile phase was 5

mM H_2SO_4 as mobile phase flowing at 0.6 ml/min. Evaporation of acetone was

significant in reactions at high temperatures (40, 55°C) and reactions involving high

acetone feed concentrations (180 mM). Peak areas so obtained were used to calculate the

concentrations of the various species using a 3 point calibration curve. A representative

chromatogram is shown in Figure 37. Isopropanol was the primary product from the

hydrogenation reactions as shown in Figure 37. Upto 1 to 2% of the acetone reacted to

form by products such as ethanol. A few peaks appeared intermittently and were most

likely intermediates; no attempt was made to identify these minor byproducts.
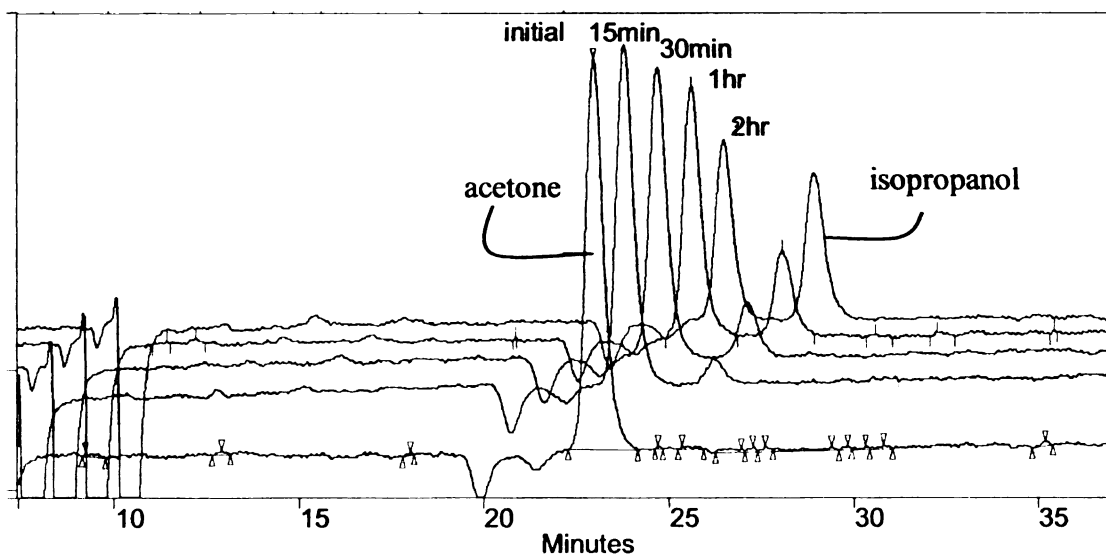
Figure 37 . Overlaid chromatograms showing decrease in acetone peak area and increase
in isopropanol peak area during the hydrogenation of acetone using tube based

microreactor with immobilized Ru/C. Flow rate 0.25 ml/min, temperature 40 °C, 650 psi hydrogen, 6 mg Ru/C in 26 inches of 800 μm tubing.

Evaporation of acetone was significant in reactions at high temperatures (40, 55°C) and reactions involving high acetone feed concentrations (180 mM). Evaporation of acetone often resulted in a lower carbon balance for the acetone and artifically high conversion values. Observed isopropanol concentrations were therefore used to back calculate acetone concentrations. Because isopropanol is the only significant product observed in batch reactions where there is no evaporation and the mass balance tallies to 100%, this methodology is valid.

There is an induction period in in the tubing reactor at 25°C that the yield of IPA in reactions at 25°C is zero at 15 minutes. This is likely because the catalyst was not prereduced prior to reaction. The setup could not, in its present form, prereduce the catalyst. Modification are possible to enable the same, however, they were not made in the present case, and therefore a suitable zero time point was assumed based on a polynomial fit of the reaction data. The fact that the reaction rate at 25°C is low enough for the data points to be linear is advantageous. This polynomial fit was also used to compare the predictions from the model at suitable time intervals and obtain the parameters giving the best fit. Where this approach has been used, primarily with data from tubing 2, the points from polynomial fit are shown alongwith the original reaction data.

5.4 Results and Discussion

Three microchannel tubular reactors with catalyst immobilized in them were used to study the hydrogenation of acetone. Three separate pieces of tubing were prepared and studied in this manner. These three reactors are detailed in Table 7.

Table 7. Charactersitics of catalytic tubing prepared and used in reactions. All tubing were PDMS with an i.d. of 800 µm.

Name	Catalyst	Length cm	Catalyst loading mg
Tubing 1	Ru/C	66	6 ± 2
Tubing 2	Ru/C	45	2 ± 1
Pd/C tubing	Pd/C	53	10 ± 4

5.4.1 Results from Tubing 1

Tubing 1 was used to compare activity of Ru/C with Pd/C, and to study the effects of temperature, catalyst loading, and acetone concentration. These are detailed in the sections to follow.

5.4.1.1 Comparison of Activity of Pd/C with Ru/C

Ru/C was found to have considerably higher activity for converting acetone to isopropanol as compared to Pd/C, as seen from Table 8 below. The material balances are low in this case because of acetone evaporation at relatively high temperature (55°C).

Table 8. Comparison of the activitiy of Pd/C and Ru/C towards the hydrogenation of acetone

Feed	Amount of catalyst; length of catalytic tubing	Time, temperature, pressure	Yield to IPA +/- 4%	% conversion of acetone	Carbon balance %
7.5 ml 5mM acetone	5 mg of 1% Pd/C 53 cm Tubing Pd/C	2 h at 55 °C, 650 psi H₂	9 ± 2%	55 %	53 %
7.5 ml 5mM acetone	6 mg of 5% Ru/C 66 cm Tubing 1	1 h at 55 °C, 650 psi H₂	66 ± 4%	87 %	77 %

5.4.1.2 Effect of Temperature

The following table (Table 9) illustrates the increase in reaction rate with increase in temperature

Table 9. Increase in reaction rate with increase in temperature, all data using Tubing 1

Feed		Time	Yield to IPA, +/- 4%	% conversion of acetone	Carbon balance %
7.5 ml 5 mM acetone	27°C 625 psi H₂	1 hour	4 ± 4%	10 %	94 %
7.5 ml 5 mM acetone	40°C 650 psi H₂	1 hour	22 ± 4%	35 %	88 %
7.5 ml 5 mM acetone	55°C 600 psi H₂	1 hour	71± 4%	90 %	78%

84

The initial rates were calculated using the one hour data points (concentration change after 1 hour divided by time). These data give an activation energy value of 91 kJ/mol (Figure 38). This value of the activation energy is on the higher side of values reported in the literature[77] of 75 kJ/mol but is close to our findings from studies of organic and amino acid hydrogenations. It should be noted in Table 9 that carbon balances again are worse at higher temperatures because of acetone evaporation.

$$y = -10918x + 24.9$$
$$R^2 = 0.99$$
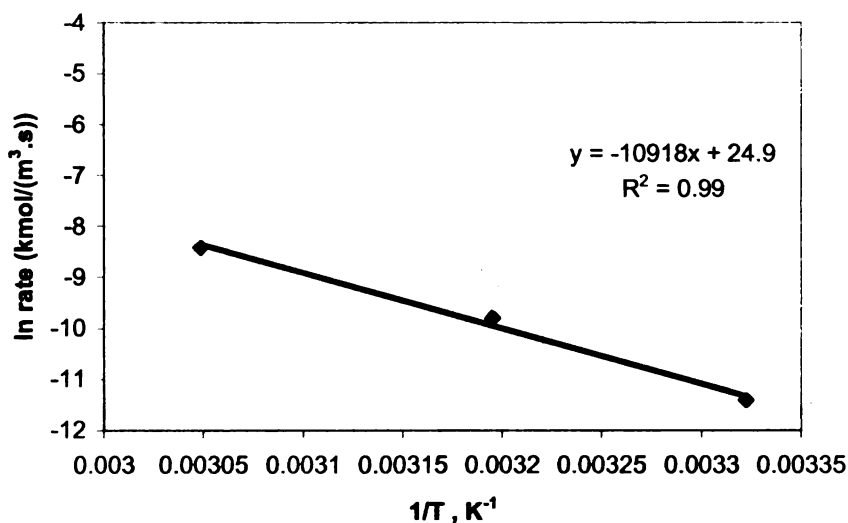
Figure 38. Activation energy for acetone hydrogenation using 1 hour data points

5.4.1.3 Effect of Catalyst Loading

To confirm that the reaction was catalytic (e.g. proportional to catalyst loading and free of mass transfer limitations), the tubing was cut in half and one section was placed back into the reactor system. This should reduce the amount of catalyst, and thus the conversion, by 50%. On reconnecting the tubing in its entirety, we expected conversion to increase back to its original value. The values in Table 10 confirm that the reaction is indeed catalytic.

Table 10. Catalytic effect of tubing length – conversion changes with amount of catalyst. All data using Tubing 1.

Feed	Length of catalytic tubing	Time, temperature, pressure	Yield to IPA +/- 4%	% conversion of acetone	Carbon balance %
7.5 ml 5mM acetone	66 cm	1 h at 40 °C, 650 psi H$_2$	22 %	35 %	84 %
7.5 ml 5mM acetone	30 cm	1 h at 40 °C, 650 psi H$_2$	9 %	16 %	92 %
7.5 ml 5mM acetone	66 cm	1 h at 40 °C, 675 psi H$_2$	24 %	35 %	90 %

5.4.1.4 Effect of Acetone Concentration

At 650 psi of hydrogen pressure, the concentration of hydrogen in water is approximately 30mM. To confirm that hydrogen was not a limiting reactant at 650 psi and 5mM acetone, reactions were run at higher concentrations of acetone, 30mM and 180 mM, while keeping the hydrogen pressure at 650 psi. As seen in Table 11, it is observed that the concentration of isopropanol formed after 1 hour at 40 °C increases with an increase in the acetone concentration even though the hydrogen concentration is kept constant at 650 psi. This confirms that hydrogen is not the limiting reactant under the reaction conditions.

Table 11. Effect of change in acetone concentration on reaction rate, all data using Tubing1

Feed	Time, temperature, pressure	H$_2$ Concn.	Conc. of IPA formed	Yield to IPA +/- 4%	% conversion of acetone	Carbon balance %
7.5 ml 5mM acetone	1 h at 40 °C, 650 psi H$_2$	30 mM	1 mM	22 %	35 %	84 %
7.5ml 30mM acetone	1 h at 40 °C, 640 psi H$_2$	30 mM	2.6 mM	8%	20 %	88 %
7.5ml 180 mM acetone	1 h at 40 °C, 640 psi H$_2$	30 mM	13 mM	8%	20 %	88 %

5.4.1.5 Kinetic Model

A simple model for the system would be a differential batch reactor with the governing equation

$$\frac{dCa}{dt} = -k(Ca)^n \qquad (1)$$

where it is assumed that the reaction kinetics can be describe by an nth order dependence on the concentration of acetone, kC_a^n. However, an accurate model of the system requires that the different components of the system be included along with equations that describe their behaviour (Figure 39).

v = 0.25 ml/min

Sample port

$$\frac{dC_A}{d\tau} = -k\, C_A$$

Microreactor
with catalyst

Volume

$V_R = 0.3ml$

HPLC
pump

C_{A1}

C_{A1}

C_{A2}

Dotted line
represents high
pressure Parr
reactor
boundary

Reservoir vial
volume 7.5 ml

700 psi
hydrogen
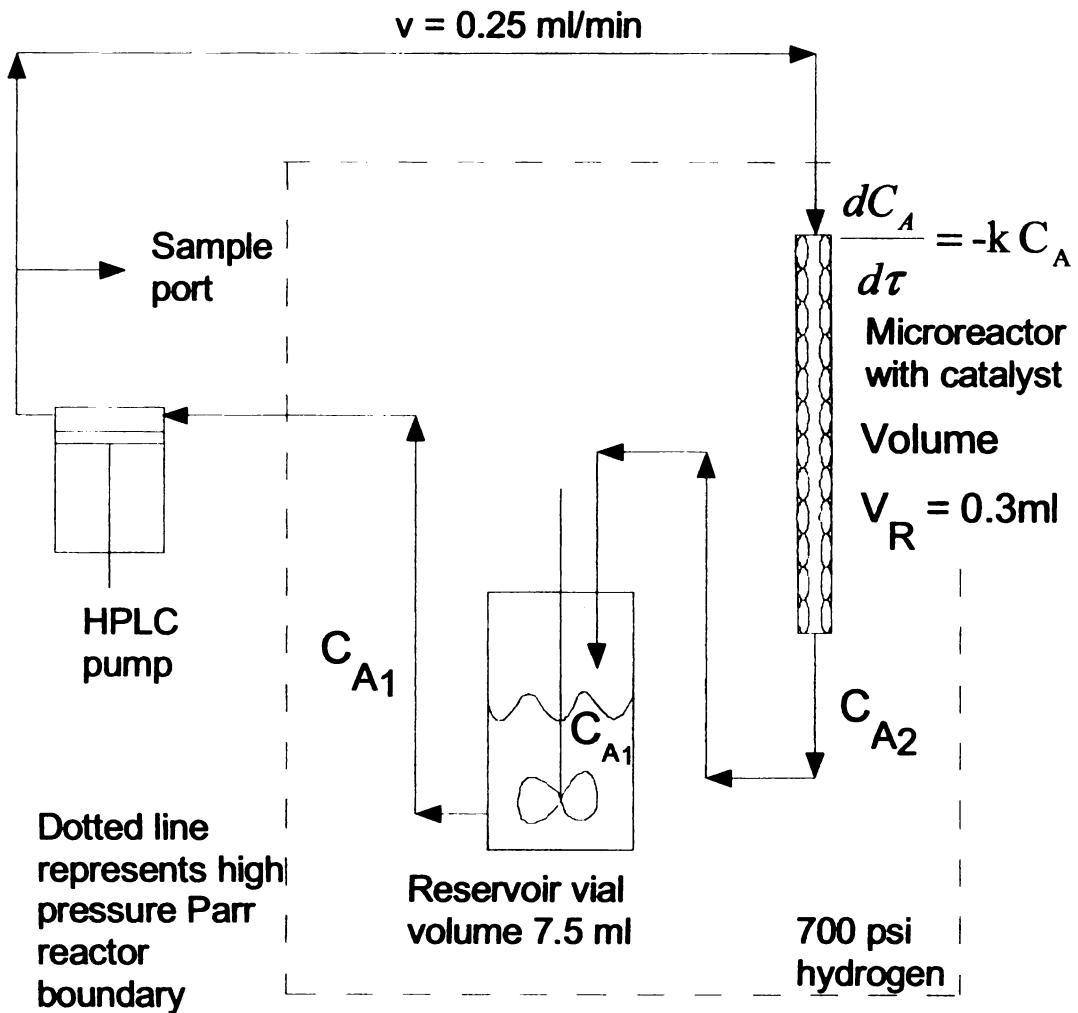
V_T = total volume = 9 ml

$$\tau = \frac{V_R}{v} = \frac{1\,\text{ml}}{0.25\,\text{ml/min}} = 4\,\text{min}$$

Figure 39. A model for the microreactor setup.

88

Accordingly, the reservoir vial containing the liquid can be modelled as a stirred tank, with the mass balance

Mass in – mass out – ~~disappearance by reaction~~ = accumulation

$$vC_{A_2} - vC_{A_1} = V_{CST}\frac{dC_{A1}}{dt} \qquad (2)$$

With residence time in the stirred tank denoted by $\tau_{CS} = \dfrac{V_{CS}}{v}$, the above equation becomes

$$\frac{dC_{A1}}{dt} = \frac{\left(C_{A2} - C_{A1}\right)}{\tau_{CS}} \qquad (3)$$

The microreactor with catalyst deposited within it can be modeled as a plug flow reactor. For such a reactor,

$$\frac{dC_{A1}}{d\tau_{PF}} = -kC_{A1}^{n} \qquad (4)$$

with the RHS again being based on the assumption that the reaction kinetics can be describe by an nth order dependence on the concentration of acetone, kC_a^{n}. Equations (1)

and (4) together can be solved to describe the variation of concentration over time in the reservoir vial. These predicted concentration profiles can be compared with experimental values obtained from a set of experiments.

For a zero and first order reaction behaviour, analytical solutions exist. In the case of a first order reaction,

$$C_{A1t} = C_{A0} \exp\left(\frac{-\left(1-e^{-k\tau}\right)}{\tau_t}\right)t \tag{5}$$

For a zero order reaction,

$$C_{A0} - C_{A1t} = \frac{k\tau_{PFR}}{\tau_{CS}}t \tag{6}$$

However these solutions described above do not describe the experimental data accurately. In the case of second order reaction kinetics, i.e.

$$\frac{dC_{A2}}{d\tau_{PF}} = -kC_{A2}^2 \tag{7}$$

an analytical solution of the plug flow (above) equation is possible yielding

$$C_{A2} = \left(\frac{1}{C_{A1}} + k\tau_{PF}\right)^{-1} \tag{8}$$

For reaction behaviour of this sort, plugging in the above equation into equation (3) for the stirred tank results in the following equation:

$$\frac{dC_{A1}}{dt} = \frac{\left(\dfrac{1}{C_{A0}} + k\tau_{PF}\right)^{-1} - C_{A0}}{\tau_{CS}} \tag{9}$$

which is not amenable to an analytical solution. Numerical integration allows calculation of the predicted concentration profile; however, this model does not give a good description of the data either, as shown in Figure 40 below.

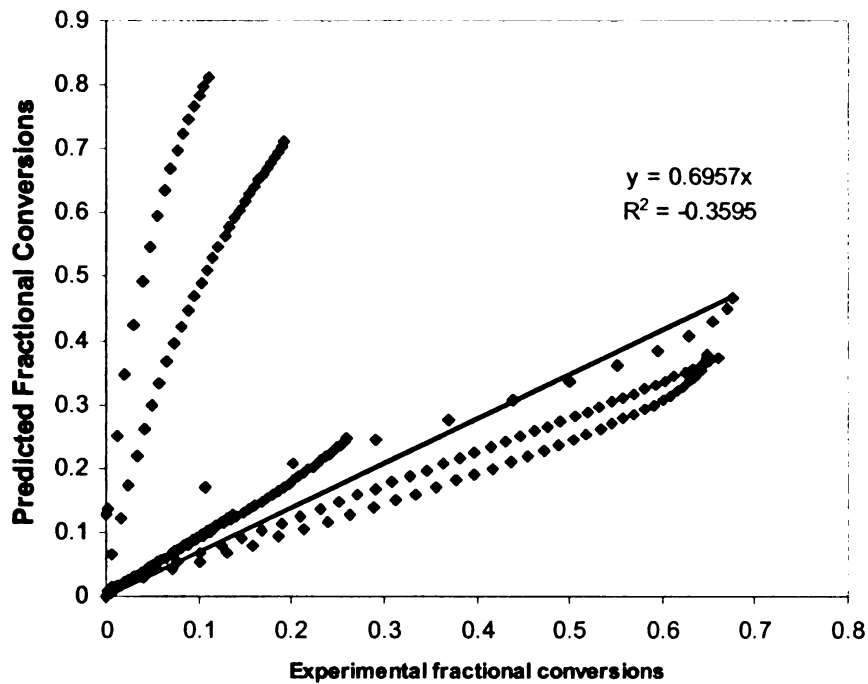Figure 40. Predicted versus experimental fractional conversions as predicted by the second order equation when plugged into the residence time model.

Most studies of acetone hydrogenation conclude that the hydrogenation of acetone follows Langmuir-Hinshelwood type kinetics, with acetone and hydrogen adsorbing on different types of active sites on the catalyst surface and then reacting to form the product

which then desorbs. Accordingly, the reaction kinetics can be described by an equation of the form

$$-r_A = \frac{k'C_A}{1 + K_A C_A} \frac{K_{H_2} C_{H_2}}{\sqrt{1 + K_{H_2} C_{H_2}}} \qquad (7)$$

where k' denotes the reaction rate constant and K_A and K_{H_2} denotes the adsorption coefficients for acetone and hydrogen on the catalyst surface respectively. If the concentration of hydrogen is maintained constant through the set of experiments, then the hydrogen related terms remain constant and can be incorporated into a composite reaction rate constant k as denoted in the expression below:

$$-r_A = \frac{k \; C_A}{1 + K_A C_A} \qquad (8)$$

When used in the PFR, the equation is

$$\frac{dC_{A2}}{d\tau_{PF}} = -\frac{kC_{A2}}{1 + K_A C_{A2}} \qquad (9)$$

which on integration yields

$$\frac{-1}{k} \ln\left(\frac{C_{A2}}{C_{A0}}\right) - \frac{K_A}{k}\left(C_{A2} - C_{A0}\right) = \tau_{PF} \qquad (10)$$

Because the solution is implicit in C_{A2}, it is more convenient to solve equation (9) numerically to obtain the concentration at the exit of the PFR and use it in equation (3) for the stirred tank. These 2 equations allow prediction of the concentration profiles using

a given set of parameter values, viz. k and K_A. The comparison of the predicted and experimental data for three different temperatures is shown in Figure 41 below:
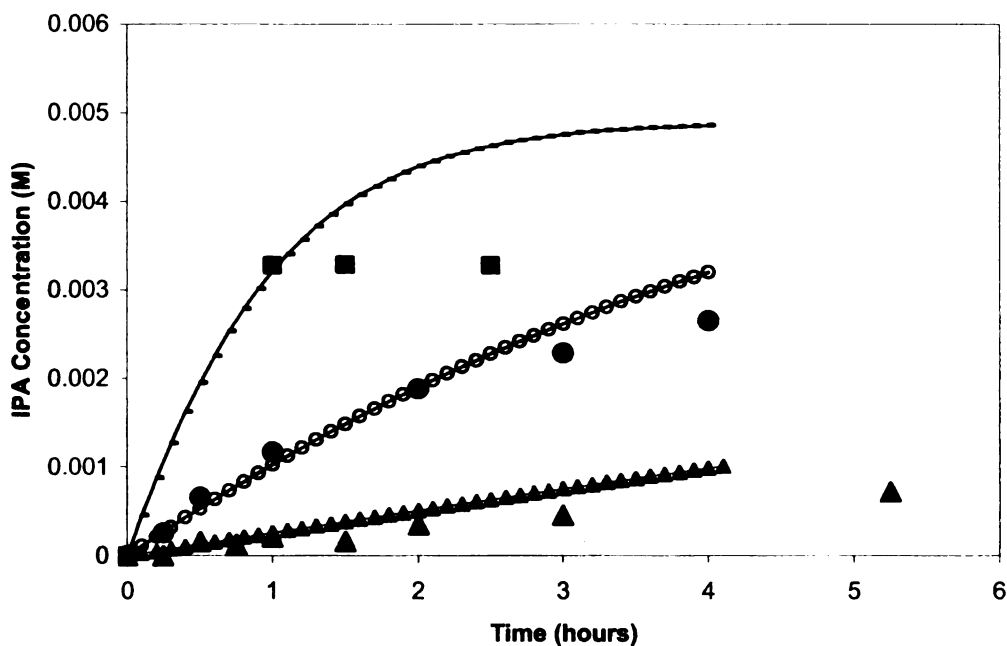
Figure 41 . Effect of temperature on the rate of formation of isopropanol. ■ denote experimental data at 55 deg C, ---■---- denote predicted data for 55 deg C; ● denote experimental data at 40 deg C, ----●----- denote predicted data for 40 deg C; ▲ denote experimental data at 27 deg C, ------▲------ denote predicted data at 27 deg C. All reactions were run in the recirculating mode at 0.25 ml/min and 650 psi H_2 with a solution volume of 7.5 ml.

To demonstrate that the reaction being observed was indeed catalytic in nature, the amount of catalyst was varied by cutting the length of tubing in half and then reconnecting the two ends. The LH model is able to predict behaviour for this set of reactions as shown in Figure 42 below.

93
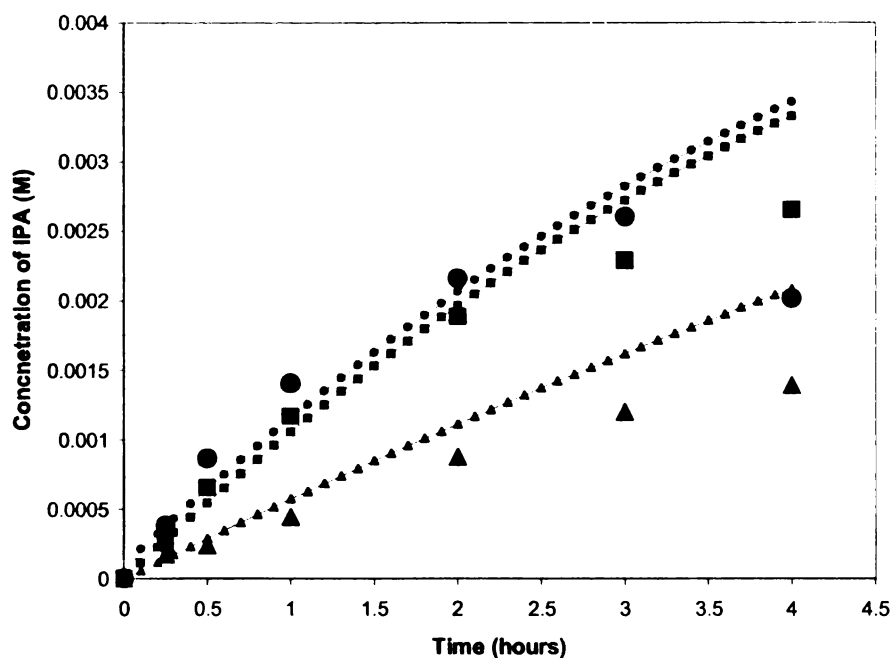
Figure 42. Effect of length of catalytic tubing on the rate of formation of isopropanol. ■ denote experimental data at 66 cm (6 mg Ru/C), ---■---- denote predicted data for 66 cm; ▲ denote experimental data for a tubing length of 33 cm (3 mg Ru/C), ----▲----- denote predicted data for 33 cm length of tubing; ● denote experimental data from a repeat experiment with 66 cm (6 mg Ru/C) length of tubing, ------●------ denote predicted data for repeat experiment with 66 cm length of tubing. All reactions were run in the recirculating mode at 0.25 ml/min, 40 deg C and 650 psi H_2 with a solution volume of 7.5 ml.

In the case of Langmuir-Hinshelwood type kinetics, in the higher concentration ranges, the reaction is likely to be zero order in the reactant concentration. Accordingly, the initial rate should not change significantly upon increasing the intial concentration of acetone from 30 mM to 180 mM. However, we see a four fold increase in the intial rate (Table 12).

Table 12 . Initial rates as affected by initial concentration of acetone.

Initial concn of acetone (mM)	Experimental initial rate mol/(lit.hr)	Initial rate if the reaction is first order mol/(lit.hr)
5	0.001	0.001
30	0.004	0.006
180	0.019	0.036

This behaviour is reflected in the predictions of the model for the 180 mM run.
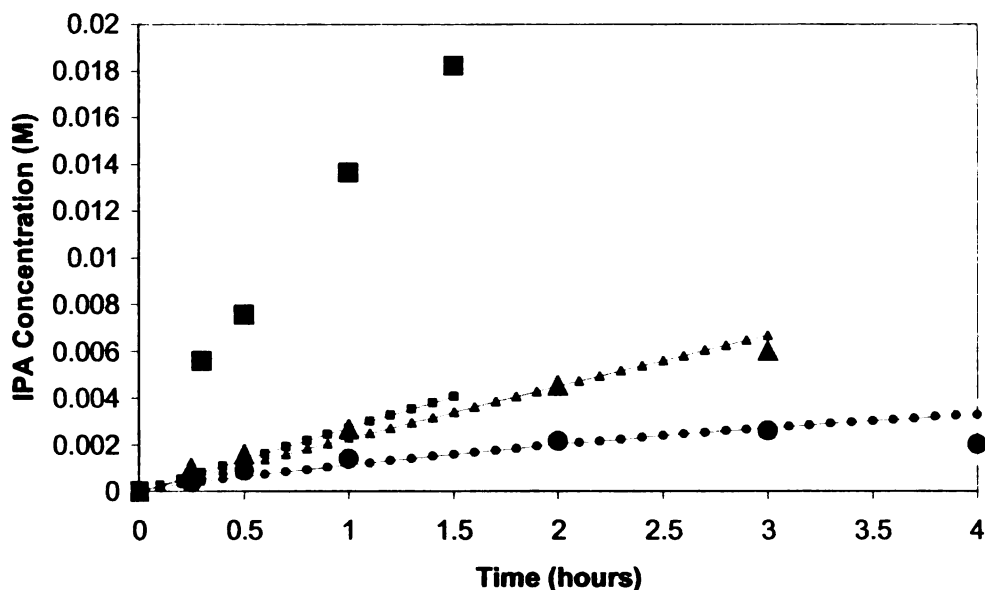
Figure 43. Effect of initial acetone concentration on the rate of formation of isopropanol. ■ denote experimental data at 180 mM initial concentration of acetone, ---■---- denote predicted data for 180 mM initial concentration of acetone; ▲ denote experimental data for a tubing length of 30 mM initial acetone concnetration, ----▲----- denote predicted data for 30 mM starting acetone concnetration; ● denote experimental data from 5 mM starting acetone conentration , ------●------ denote predicted data for repeat experiment with 5 mM intial acetone concentration. All reactions were run in the recirculating mode at 0.25 ml/min, 40 deg C and 650 psi H_2 with a solution volume of 7.5 ml.

The parameters obtained from least squares regression which give the best fit for the model are listed in Table 13 below:

Table 13. Parameter values giving best fit for the experimental data from Tubing1.

Parameter	Units	Value
k_{298}	m^3 solution / (gmcat. s)	2.25×10^{-8}
K_A	$m^3/kmol$	138
ΔE	kJ/mol	90

5.4.2 Results From Tubing 2

In order to study the effect of acetone concentration at a different catalyst loading, a fresh piece of tubing was prepared. This piece of 800 μm i.d. tubing was approximately 45 cm long and had 2 mg of Ru/C immobilized in it. Reactions were run at 25 deg C and 650 psi hydrogen at 0.25 ml/min.

5.4.2.1. Effect of acetone concentration

Reactions were starting with feed acetone concentrations of 3, 5, 9, 30 and 180 mM. The results of these runs are summarized in Figure 44.

Figure 44. Data from tubing 2, 2mg of Ru/C, at 25°C, in recirculating mode at 0.25 ml/min under 650 psi hydrogen. Each line represents concentration profile of isopropanol based on a different feed concentration.

As can be seen in Figure 44, an increase in the feed acetone concentration results in an increase in the net yield of isopropanol after 1 hour. Figure 45 shows the conversion vs. time plots normalized to a zero time of reaction; this accounts for the induction period observed at the low reaction temperature.

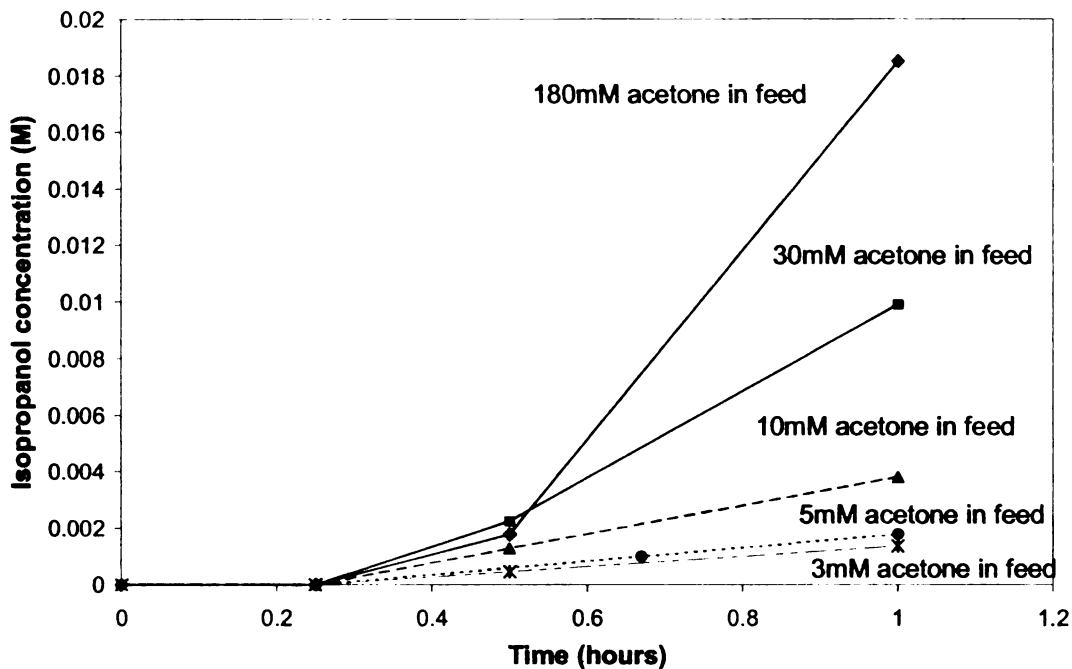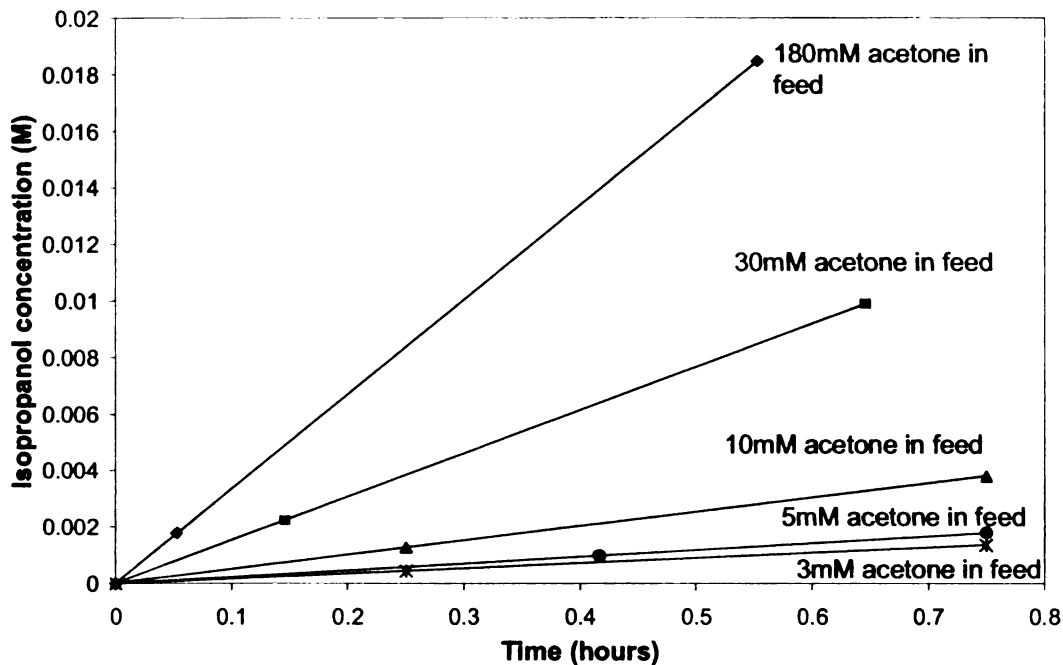Figure 45. Data from tubing 2, 2mg of Ru/C, at 25°C, in recirculating mode at 0.25 ml/min under 650 psi hydrogen. A polynomial fit has been used to estimate the start of reaction (time = zero). Reaction volume = 7.5 ml.

Figure 46 shows the effect of change in acetone concentration of feed on the intial rate of formation of isopropanol.

dci/dt (mol/(hr.lit))

0.04
0.035
0.03
0.025
0.02
0.015
0.01
0.005
0

0   20   40   60   80   100   120   140   160   180   200

Initial acetone concentration (mM)
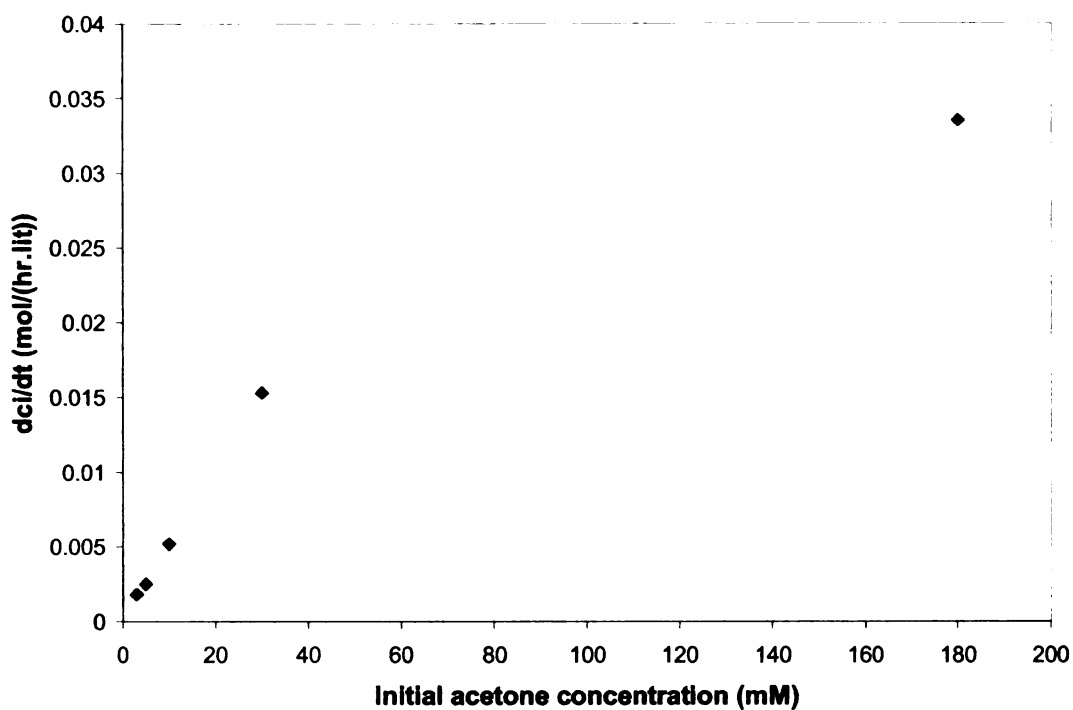
Figure 46. Effect of acetone concentration in feed on reaction rate as seen in data set 2 with tubing 2. 2mg of Ru/C, at 25°C, in recirculating mode at 0.25 ml/min under 650 psi hydrogen. Reaction solution volume = 7.5 ml.

5.4.2.2 Kinetic Model

The data set from polynomial fits for Tubing #2 was tested for fit using the Langmuir-Hinshelwood residence time model used for data set 1 (Equations 3 and 9). As can be seen from Figure 47 below, the model predicts experimental data with an average error of ± 2%.
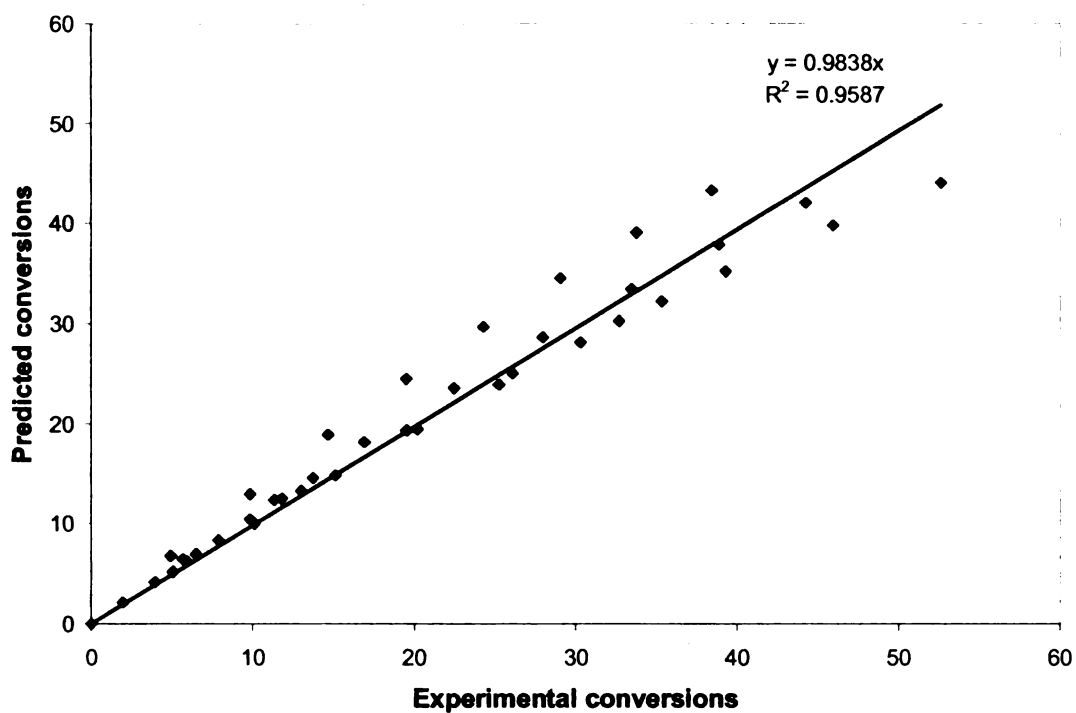
Figure 47. Parity plot comparing predicted and experimental conversions. Experimental data are from polynomial fits to data from set 2. Predictions are output from Langmuir-Hinshelwood residence time model.

The parameters giving optimum fit are listed in Table 14 .

Table 14. Parameters giving best fit for data from Tubing 2

Parameter	Units	Value
k_{298}	m^3 solution / (gmcat. s)	1.32×10^{-6}
K_A	m^3/kmol	18

100

5.4.2.3 Mass Transfer Analysis

The Weisz-Prater criterion[78] was applied to calculate the observable modulus for acetone and hydrogen inside the catalyst pores and thus gain an estimate of the role played by mass transfer inside the pores of the catalyst particles. Sample calculations for the observable modulus for acetone are shown below.

The observable moduls is calculated as per

$$\eta\phi^2 = \frac{-R_G L^2}{D_e C_B} \tag{11}$$

For a reaction with 180 mM acetone at 25 deg C and 650 psi hydrogen with the recirculating system, the values are as follows:

- Rate of reaction

$$-R_G = 0.007 \ \frac{moles.reacted}{lit.solution} \times 0.0075 \ lit\ solution \times \frac{1}{0.01 gmcat} \times \frac{1}{0.5 \times 3600 \sec}$$

$$-R_G = 2.91 \times 10^{-6} \ \frac{mol}{gmcat \times \sec} \times 1.2 \ \frac{gmcat}{cm^3 cat}$$

$$-R_G = 3.50 \times 10^{-6} \ \frac{mol}{cm^3 cat \times \sec}$$

- The diffusivities of hydrogen and acetone in water were calculated using the Wilke-Chang[79] correlation:

$$D_{acetone-H_2O} = 7.4 \times 10^{-8} \ \frac{T\left(\psi_{H_2O} M_{H_2O}\right)^{0.5}}{\mu V_{acetone}^{0.6}}$$

where

T = absolute temperature [°K] = 298 K

ψ_{H_2O} = an association parameter for the solvent water = 2.26

M_{H_2O} = molecular weight of water = 18 g/mole

μ = viscosity of water in centipoises = 0.6552 cP

$V_{acetone}$ = molar volume of acetone = 75 cm^3/gm-mole

This gives a value of diffusivity of acetone in water as

$$D_{acetone-H_2O} = 1.69 \times 10^{-5} \ \frac{cm^2 fluid}{sec}$$

The effective diffusivity D_e takes into account the porosity of the catalyst

particles

$$D_e = D_{acetone-H_2O} \times \varepsilon^2$$

where ε = porosity of the catalyst $\approx$ 0.6

Hence, for acetone in water, $D_e = 5.63 \times 10^{-6} \ \dfrac{cm^3 fluid}{cmcat \times sec}$

- Concentration of acetone in water

$$C_B = 0.00018 \ \frac{mol}{cm^3 fluid}$$

- The characteristic length L of the spherical catalyst particle is D_p/6 where Dp is the

  diameter of the particles, in this case 150 μm. Thus

  $L = 0.0025 \ cm \ cat$

Using the above values,

$$\eta\phi^2_{acetone} = 0.022$$

102

- For hydrogen in water, the value of the diffusivity changes accordingly:

$$D_{H_2-H_2O} = 7.4 \times 10^{-8} \frac{T\left(\psi_{H_2O} M_{H_2O}\right)^{0.5}}{\mu V_{H_2}^{0.6}}$$

where

V_{H_2} = molar volume of hydrogen = 20.82 cm^3/gm-mole

The value for diffusivity of hydrogen in water works out to

$$D_{H_2-H_2O} = 2.63 \times 10^{-5} \frac{cm^2 \, fluid}{sec}$$

The effective diffusivity takes into account the porosity of the catalyst particles

$$D_e = D_{acetone-H_2O} \times \varepsilon^2$$

where ε = porosity of the catalyst ≈ 0.6

Hence, for hydrogen in water, $D_e = 8.71 \times 10^{-6} \dfrac{cm^3 \, fluid}{cmcat \times sec}$

For the values

- $-R_G = 2.45 \times 10^{-6} \dfrac{mol}{cm^3 cat \times sec}$

- $L = 0.0025 \, cm \, cat$

- $C_B = 0.00003 \dfrac{mol}{cm^3 \, fluid}$

the value of the modulus works out to be

$$\eta \phi^2{}_{H_2} = 0.06$$

Results from tubing2   Observable modulus

Sr. no	volume	acetone conc at time 0	temperature	approx. catalyst (RuC) loading (Tubing 2)	H2 concn	Time	Concn of IPA formed	% yld	M blce	Rg mol/(cm³cat.s)	ηφ² acetone	ηφ² H2	φ_A	η_A	R intrinsic mol/(cm³cat.s)
1	7.5 ml	3 mM	25 deg C	2 mg	30 mM	1 h	1.4 mM	46%	95%	1.75E-06	0.92	0.0418	1.1	0.72	2.44E-06
2	7.5 ml	5 mM	25 deg C	2 mg	30 mM	1 h	1.8 mM	32%	108%	2.25E-06	0.71	0.0537	1	0.78	2.90E-06
3	7.5 ml	10 mM	25 deg C	2 mg	30 mM	1 h	3.8 mM	37%	103%	4.75E-06	0.75	0.1132	1	0.73	6.53E-06
4	7.5 ml	30 mM	25 deg C	2 mg	30 mM	1 h	10 mM	32%	96%	1.25E-05	0.66	0.2932	0.9	0.79	1.58E-05
5	7.5 ml	180 mM	25 deg C	2 mg	30 mM	1 h	18.4 mM	10%	95%	2.25E-05	0.19	0.5385	0.5	0.94	2.40E-05
6 once through	6.5 ml	9 mM	25 deg C	2 mg	30 mM	40 min	5.5 mM average	55%	110%	8.94E-06	1.56	0.2134	1.7	0.56	1.60E-05
Batch runs															
7	7.5 ml	180 mM	40 to 50 deg C	8.6 mg	30 mM	30 min	53 mM	31%	102%	3.08E-05	temp not constant				
8	7.5 ml	9 mM	25 deg C	8.5 mg	30 mM	30 min	6.5 mM	73%	104%	3.82E-06	0.72	0.0914	1	0.77	4.94E-06
9	7.5 ml	180 mM	25 deg C	10 mg	30 mM	30 min	7 mM	4%	97%	3.50E-06	0.02	0.0342	0.1	0.99	3.52E-06
Old batch runs															
10	7.5 ml	5 mM	40 deg C	11 mg	30 mM	15 min	2.7 mM	46%	100%	2.45E-06	0.6	0.0552	0.9	0.81	3.03E-06
11	7.5 ml	180 mM	40 to 50 deg C	6 mg	30 mM	30 min	2.5 mM	1.30%	98%	stirrer impeded by filter?					

Table 15. Mass Transfer Analysis and Observable Modulii Values for Acetone Hydrogenation

A summary of such calculations for the 2nd set of reactions is shown in Table 15 above.

It can be seen that the reaction rates lie in a regime where diffusion within the pores reduces the observed reaction rate by 25% as compared to the intrinsic reaction rate. Higher acetone concentrations and lower reaction temperatures can reduce diffusional limitations.

5.5 Conclusion

An immobilization technique to deposit catalyst in microchannels was developed. The technique was used in conjunction with a low volume high pressure recirculating system to demonstrate catalytic hydrogenation of acetone. The effect of various parameters on the reaction rate was studied, and it was demonstrated that the reaction is catalytic in nature and that hydrogen is not the limiting reactant under standard reaction conditions. Comparison with an analogous batch setup demonstrates that the catalyst exhibits similar activities in both the batch and continuous modes of operation. The setup can be easily modified to act as a one pass flow through system and thus has potential application as a high throughput catalyst screening system. A small amount of catalyst, of the order of a few milligrams can be used to study catalytic reactions, which can be very advantageous when screening catalysts.

Some of the advantages in using a PDMS tube as a microreactor instead of a PDMS-glass microreactor are mentioned below. Connections between the tubing and flow loop are considerably simpler and more robust as compared to connections between a composite microreactor and the flow loop. This saves a lot of development time as a

large proportion of prototypes failed due to leakage at the interface with the flow loop. Because glass and PDMS have different coefficients of thermal expansion, rapid heating of a glass-PDMS microreactor can cause strain at the PDMS-glass bond. This can cause distortion of the flow path and in some cases breakage of the microreactor. In the case of PDMS tubing, there are no such problems and the tubing can be heated to temperatures as high as 200 °C. It is also possible to introduce more catalytic tubing into the flow path and thus check for the effect of increase in catalyst loading without having to discard the original microreactor, as would be the case with the PDMS-glass microreactor.

Nomenclature

τ_{CS} = Space time in stirred tank = 1920 (m^3 reactor . sec)/m^3 solution

τ_{PF} – Space time in catalytic tubing (PFR) = 72 (m^3 reactor . sec)/m^3 solution

C_{A1} = concentration of acetone in the stirred tank at any time t, kmol/m^3

C_{A2} = Concentration of acetone at the exit of catalytic tubing at any time t, kmol/m^3

k = Composite reaction rate constant, s^{-1}

K_A = adsorption coefficient for acetone, m^3/kmol

v = flow rate of reaction mixture, m^3/s = 4.2 × 10^{-9} m^3/s

V_{CST} = Volume of stirred tank = 8 × 10^{-6} m^3

References

77. R.Alcala, J. Greeley, M. Mavrikakis, and J. A. Dumesic, *J. Chem. Phys.*, 2002, **116**, 20, 8973-8980

78. P. Weisz, C. Prater, *Adv. Catal.* 1954, **6**, 143-196.

79. C. Wilke, P. Chang, *AIChE J.* 1955, **1**, 264-270